Cell

Short article

Inheritance of acquired adaptive cold tolerance in rice through DNA methylation

Graphical abstract

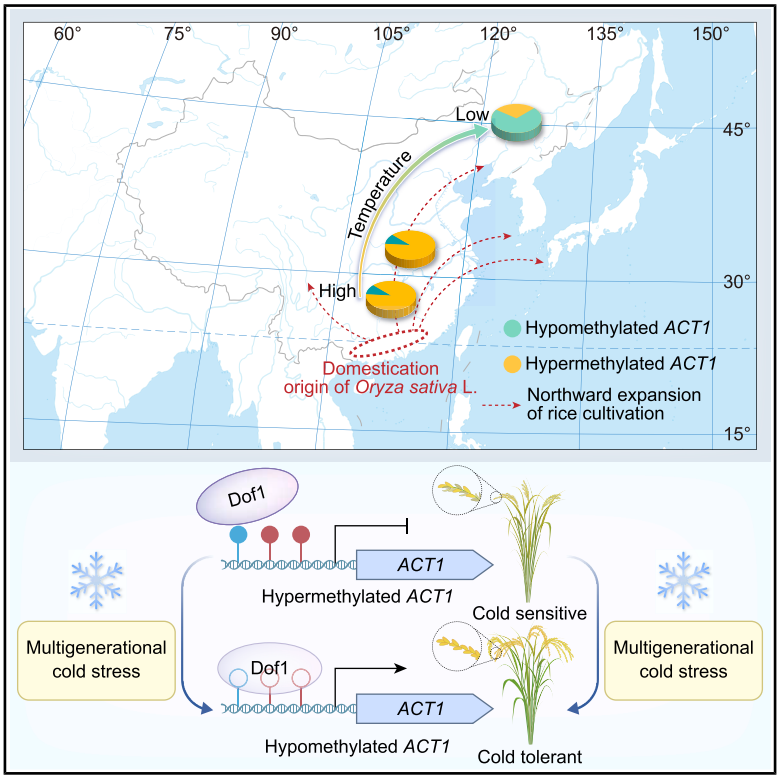

Highlights

- Recurrent cold stress during reproduction induces heritable cold tolerance in rice
- Cold-induced DNA demethylation of *ACT1* mediates cold tolerance acquisition
- Natural variation in *ACT1* DNA methylation causes differential Dof1 binding
- Hypomethylated *ACT1* epiallele enhances rice adaptation to high-latitudinal regions

Authors

Xianwei Song, Shanjie Tang, Hui Liu, ..., Shukun Jiang, Xian Deng, Xiaofeng Cao

Correspondence

xwsong@genetics.ac.cn (X.S.), xfcao@genetics.ac.cn (X.C.)

In brief

Multigenerational cold stress induces heritable *ACT1* promoter hypomethylation, enabling rice to acquire cold tolerance for high-latitude adaptation.

Song et al., 2025, Cell *188*, 4213–4224
August 7, 2025
https://doi.org/10.1016/j.cell.2025.04.036

CellPress

Cell

CellPress
OPEN ACCESS

Short article

Inheritance of acquired adaptive cold tolerance in rice through DNA methylation

Xianwei Song,[1,2,10,*] Shanjie Tang,[1,6,10] Hui Liu,[3,9,10] Ying Meng,[4] Haofei Luo,[1] Bao Wang,[5] Xiu-Li Hou,[1] Bin Yan,[1] Chao Yang,[1] Zhenhua Guo,[1] Lizhi Wang,[4] Shukun Jiang,[4] Xian Deng,[1,8] and Xiaofeng Cao[1,7,8,11,*]

[1]Institute of Genetics and Developmental Biology, Chinese Academy of Sciences, Beijing 100101, China
[2]State Key Laboratory of Seed Innovation, Institute of Genetics and Developmental Biology, Chinese Academy of Sciences, Beijing 100101, China
[3]Germplasm Bank of Wild Species & Yunnan Key Laboratory of Crop Wild Relatives Omics, Kunming Institute of Botany, Chinese Academy of Sciences, Kunming 650201, China
[4]Institute of Crop Cultivation and Tillage, Heilongjiang Academy of Agricultural Sciences, Harbin 150086, China
[5]Shaanxi Key Laboratory of Qinling Ecological Intelligent Monitoring and Protection, School of Ecology and Environment, Northwestern Polytechnical University, Xi'an 710072, China
[6]College of Life Sciences, University of the Chinese Academy of Sciences, Beijing 100039, China
[7]College of Advanced Agricultural Sciences, University of Chinese Academy of Sciences, Beijing 100049, China
[8]Laboratory of Advanced Breeding Technologies, Institute of Genetics and Developmental Biology, Chinese Academy of Sciences, Beijing 100101, China
[9]Key Laboratory of Plant Diversity and Specialty Crops, Chinese Academy of Sciences, Beijing 100093, China
[10]These authors contributed equally
[11]Lead contact
*Correspondence: xwsong@genetics.ac.cn (X.S.), xfcao@genetics.ac.cn (X.C.)
https://doi.org/10.1016/j.cell.2025.04.036

SUMMARY

Epigenetic pathways could provide a mechanistic explanation for the inheritance of acquired characteristics, as proposed by Lamarck in 1802, but epigenetic alterations that endow adaptive hereditary traits have rarely been observed. Here, in cultivated Asian rice (*Oryza sativa* L.), we identified an epiallele conferring acquired and heritable cold tolerance, an adaptive trait enabling northward spread from its tropical origins. We subjected cold-sensitive rice to multigenerational cold stress and identified a line with acquired stable inheritance of cold tolerance. DNA-hypomethylation variation in the *acquired cold tolerance 1* (*ACT1*) promoter region rendered its expression insensitive to cold. This change is, in large part, responsible for the acquired cold tolerance, as confirmed by DNA-methylation editing. Natural variation in *ACT1* DNA hypomethylation is associated with cold tolerance and rice geographic distribution. Hypomethylation at *ACT1* triggers adaptive cold tolerance, presenting a route to epigenetic-variation-driven inheritance of acquired characteristics.

INTRODUCTION

The idea that the environment can directly drive adaptive phenotype changes in a heritable manner is known as the inheritance of acquired characteristics. Adaptability and hereditary stability are two key properties of this,[1] with several inheritance-of-acquired-characteristics-related phenomena with adaptive features known.[2–4] Owing to the lack of direct molecular evidence, a compelling demonstration of inheritance of acquired characteristics remains elusive.[5] Epigenetic mechanisms, including DNA methylation and small RNAs, are linked to environmentally induced phenotype changes,[6–12] and DNA-methylation-associated epialleles can mediate inherited phenotypes in plants.[13–19] However, these changes have not been shown to have adaptive significance while retaining hereditary stability, and therefore demonstration of inheritance of acquired characteristics awaits.

Here, we analyzed cold tolerance, an adaptive trait of Asian rice, enabling its northward spread away from its tropical origin.[20,21] We identified and genetically confirmed that DNA hypomethylation in the *acquired cold tolerance 1* (*ACT1*) gene, induced by multigenerational cold stress, promotes both cold-tolerance acquisition and its stable inheritance. Natural variation in DNA methylation at *ACT1* correlates with cold tolerance and geographic distribution of rice. We demonstrate that environmentally induced epigenetic variation contributes to the inheritance of an acquired characteristic.

RESULTS

Multigenerational cold stress triggers heritable cold tolerance

During the northward range expansion of rice, cold tolerance was acquired to adapt to low-temperature environments.[22] To investigate the mechanism responsible for this, we designed a cold-acclimation experiment to screen for variants with acquired and heritable cold tolerance. Male reproductive development is

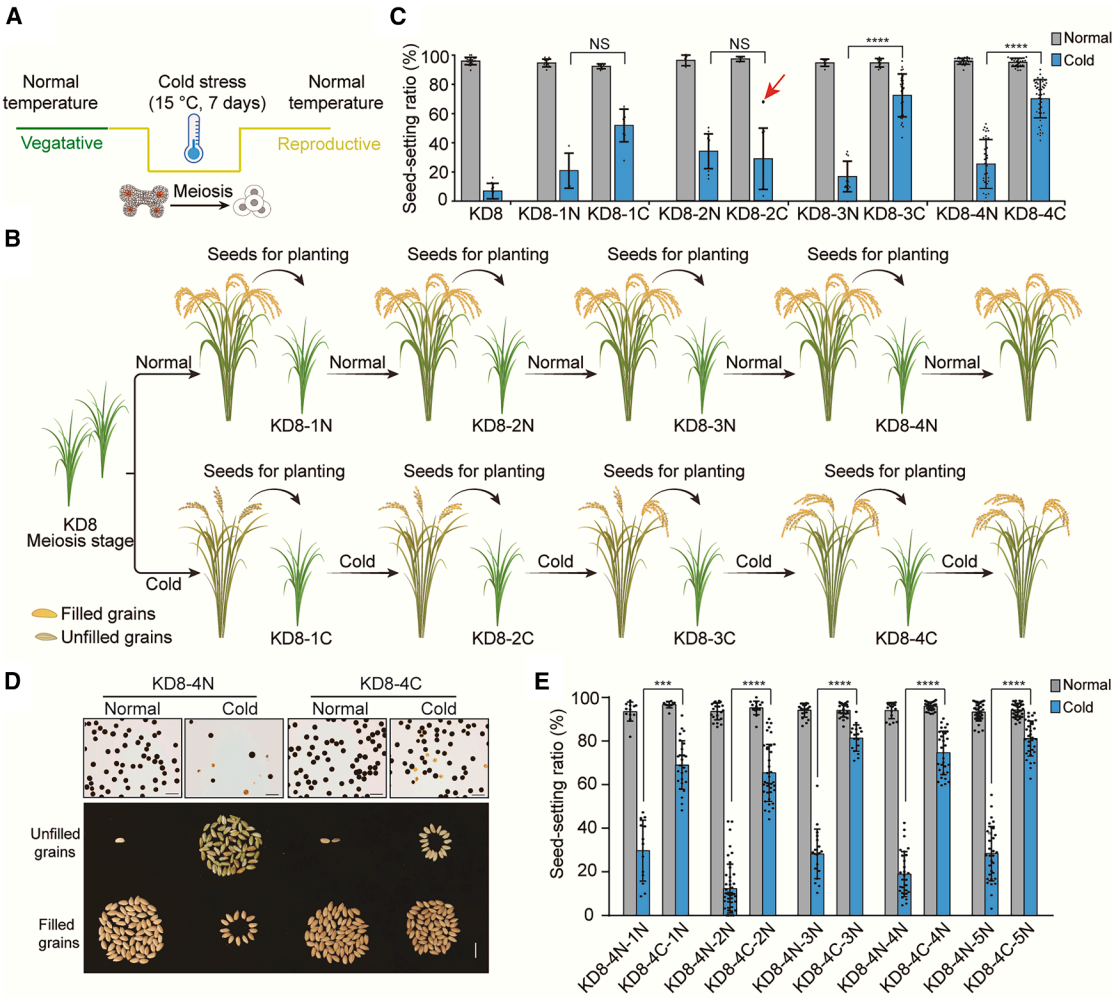

Figure 1. Cold-stress-driven acquisition and stable inheritance of cold tolerance in rice

(A) Schematic of cold treatment during the meiotic stage in rice. The experiment was conducted in Harbin, China, from May to October each year, using potted plants. The normal temperature corresponds to the natural ambient temperature in the region, while the cold treatment was carried out in a phytotron under natural lighting conditions.

(B) Screening for cold-tolerance acquisition generation by generation. N, normal temperature; C, cold stress, 1C–4C, the generation numbers experiencing cold stress.

(C) Seed-setting ratio of KD8 and its progeny as developed in (B) at normal and cold temperatures. The red arrow in the KD8-2C profile indicates the panicle from which its self-progenies were used for further cold treatment. ****$p < 0.0001$; ns, non-significant, Wilcoxon matched-pairs signed rank test.

(D) Pollen fertility (top) and filled or unfilled grains (bottom) of representative panicles from KD8-4N and KD8-4C plants grown under normal and cold temperatures. Scale bars, 100 μm (pollen) and 1 cm (grain).

(E) Seed-setting ratio of KD8-4N and KD8-4C inbred lines over the successive five generations without cold stress, under normal and cold temperatures. 1N–5N indicate the generation numbers at normal temperature. ***$p < 0.001$; ****$p < 0.0001$, Wilcoxon matched-pairs signed rank test.

See also Figure S1 and Table S1.

highly sensitive to cold.[23–25] We developed a cold-tolerance evaluation system by subjecting meiotic-stage plants to cold that affects spikelet fertility and yield[26,27] (Figures 1A, S1A, and S1B). We distinguished cold tolerance among 31 varieties/landraces from northern China, with KenDao8 (KD8) being very cold sensitive (Figures S1C–S1E; Table S1). KD8 was subjected to multigenerational cold stress (Figure 1B). At each generation, we selected panicles with increased cold tolerance, the seeds from which were collected, planted, and subjected to further rounds of stress. A panicle with a high seed-setting ratio was observed after the second round of cold stress (Figure 1C). Seeds planted from this cold-tolerant panicle and subjected to a third round of cold treatment yielded plants (designated "KD8-3C" for three generations of cold, "C") with increased seed set (Figure 1C). This cold-tolerance acquisition, inferred by increased seed set, persisted in the progeny from KD8-3C (KD8-4C, Figures 1C and 1D). Cold tolerance can be acquired within three generations of cold stress at the meiotic stage.

Hereditary stability is a key feature of inheritance of acquired characteristics.[1] To explore this, we developed inbred lines in

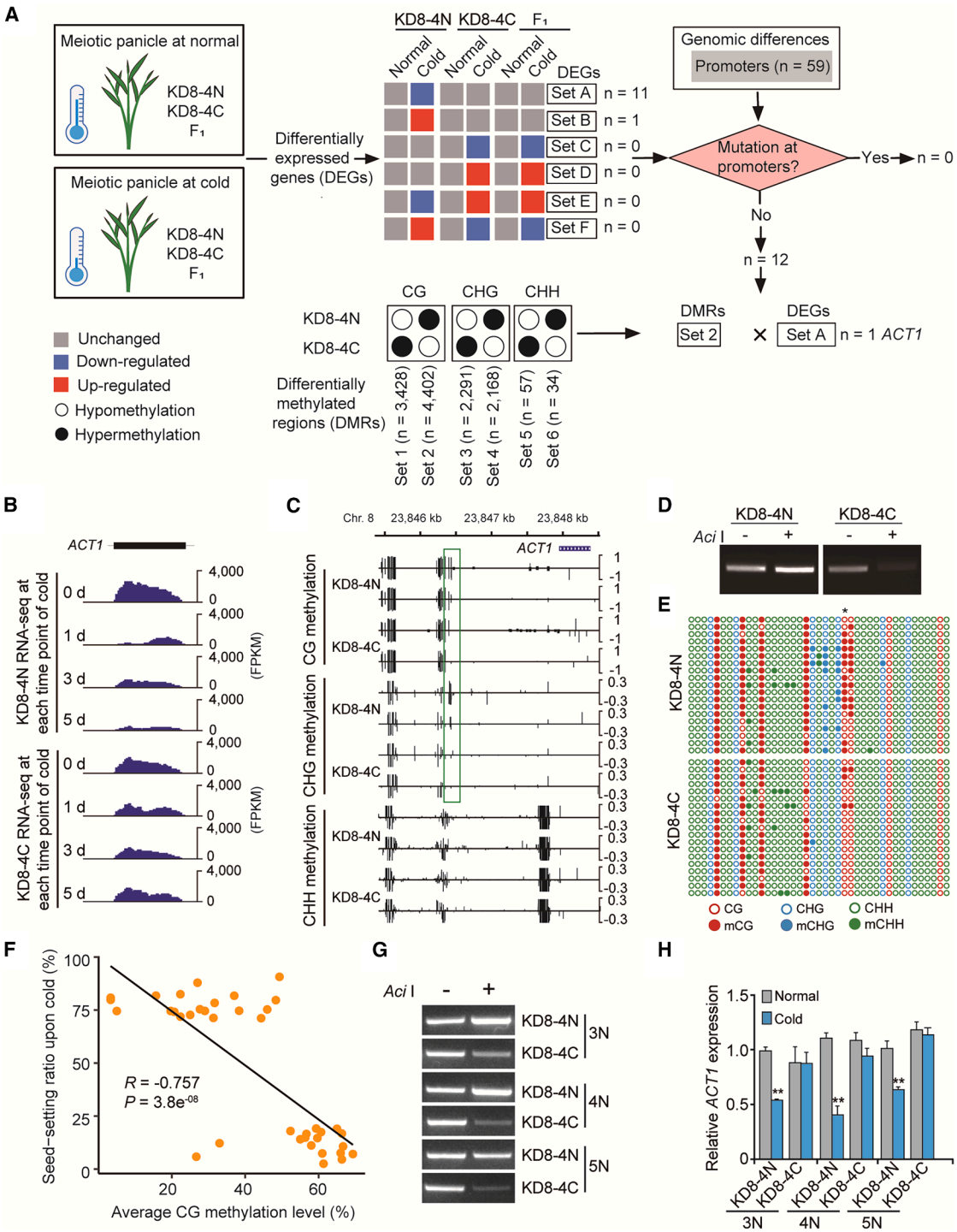

Figure 2. The *ACT1* epiallele is associated with cold-tolerance acquisition

(A) Candidate-gene identification by combined analyses of genomes, transcriptomes, and DNA methylomes. *n*, number of genes or DMRs.

(B) RNA-seq read coverage of *ACT1* in KD8-4N and KD8-4C at the indicated cold-treatment time points. FPKM, fragments per kilobase per million.

(C) DNA-methylation status of the *ACT1* region revealed by whole-genome bisulfite sequencing. The green rectangle indicates the methylation region that varies between KD8-4N and KD8-4C.

(D and E) Confirmation of *ACT1* DNA-methylation variation by Chop-PCR (D) and bisulfite sequencing (E). The asterisk in (E) indicates the *Aci*I site. Each circle represents a methylated (solid) or non-methylated (empty) cytosine. Sequence contexts of cytosine are distinguished by red for CG, blue for CHG, and green for CHH (H = C, T or A). Each row represents an independent clone.

(legend continued on next page)

parallel over the successive five generations for KD8-4N controls grown under normal ("N") temperatures and KD8-4C. Upon cold treatment, the seed-setting ratio of offspring at each generation was consistently maintained at 70%–80%, higher than the progenies of KD8-4N developed in parallel (Figure 1E). All F_1 panicles derived from reciprocal crosses between KD8-4C and KD8-4N exhibited high seed-setting ratios upon cold stress (Figure S1F). The loci/locus controlling the acquired cold tolerance behaves in a dominant manner and can be transgenerationally inherited for at least five generations without a cold stimulus.

Cold tolerance is controlled by dominant epigenetic variation

Sequencing and assembly of KD8-4C and KD8-4N genomes revealed perfect collinearity between them (Figure S2A), with only 877 SNPs/insertions or deletions (indels) identified, most of which are in repeat regions: 745 in transposable-element regions, 32 in intergenic regions, 59 in promoters, and 41 in gene bodies, with only one causing an altered amino acid sequence (a 3-bp deletion in KD8-4C) for *Os02g0776800* (Figure S2B). This in-frame mutation shows a statistically non-significant correlation with cold tolerance among the F_2 population generated by reciprocal crosses between KD8-4N and KD8-4C (Figure S2C), suggesting it is not responsible for the acquired trait in KD8-4C.

We next searched candidate genes displaying differential expression from KD8-4N, KD8-4C, and their F_1 progeny at meiotic-stage panicles subjected to cold stress for 0, 1, 3, and 5 days. Principal-component analysis suggested that expression changes are strongly affected by cold treatment (Figure S2D). Based on the dominant nature of the acquired cold-tolerance trait, we hypothesized that the candidate genes would show similar expression patterns between KD8-4C and F_1 progeny, but different from KD8-4N, when responding to cold. Following this, 12 candidate genes were identified (Figures 2A and S2E). The 59 SNPs/indels identified in promoter regions between KD8-4N and KD8-4C are not located in these 12 genes, suggesting that genetic variation might account less for acquired cold tolerance (Figure 2A).

We then explored epigenetic variation in these 12 differentially expressed genes. DNA methylation occurs in CG, CHG (H = A, C, T), and CHH contexts in plants and is the most prevalent epigenetic mark.[28] Methylation at CG (mCG) and CHG (mCHG) levels were similar between KD8-4N and KD8-4C, while methylation at CHH (mCHH) levels showed a small increase in KD8-4C (Figure S2F). A total of 7,830 CG, 4,459 CHG, and 91 CHH differentially methylated regions (DMRs) were identified between the KD8-4N and KD8-4C genomes. Of these, 56.2% CG, 48.6% CHG, and 37.3% CHH regions were hypomethylated in KD8-4C, compared with KD8-4N (Figures 2A and S2G). Among the 12 candidate genes, only 1, *Os08g0482300*, contained a DMR in KD8-4C. We therefore named it *ACT1*.

DNA hypomethylation at *ACT1* enables cold tolerance

ACT1 expression was decreased at 1, 3, and 5 days of cold treatment in KD8-4N but showed less changes in KD8-4C and F_1 progeny (Figures 2B and S2E). We did not detect any nucleotide variation in the *ACT1* gene body and promoter region across KD8-4N and KD8-4C. However, DNA hypomethylation was observed in a contiguous 37-bp region from −1,549 to −1,513 bp upstream of the *ACT1* transcriptional start site in KD8-4C. This region contains three CG and three CHG sites (Figure 2C), which were confirmed using methylation-sensitive enzyme digestion followed by PCR (Chop-PCR) (Figure 2D) and bisulfite sequencing (Figure 2E).

To explore whether the *ACT1* hypomethylation allele is transgenerationally inherited and associated with cold tolerance, we ran a correlation analysis between *ACT1* DNA methylation and cold tolerance among the progenies from the F_2 population generated by reciprocal crosses between KD8-4N and KD8-4C. Upon cold, seed-setting ratios exhibited a continuous distribution (Figure S2H), suggesting that multiple loci contribute to the acquired cold-tolerance traits. We hypothesized that if the *ACT1* hypomethylated epiallele is a major contributor to the phenotype, it will be enriched in F_2 cold-tolerant individuals, while hypermethylated *ACT1* will be enriched in cold-sensitive individuals. To test this, we analyzed *ACT1* methylation in 18 cold-sensitive plants (with cold tolerance similar to or less than that of KD8-4N) and 20 cold-tolerant ones (with cold tolerance similar to or more than that of KD8-4C) (Figure S2H; Table S2). The *ACT1* hypomethylation allele is prevalent in the cold-tolerant group but less common in the cold-sensitive group, with a strong negative correlation observed between *ACT1* methylation level and cold tolerance (Pearson's $R = -0.757$, $p = 3.8e^{-8}$ for CG; $R = -0.71$, $p = 5.8e^{-7}$ for CHG; Figures 2F and S2I). DNA hypomethylation and cold-insensitive *ACT1* expression persisted in higher generations of KD8-4C inbred lines (Figures 2G and 2H). Thus, cold-induced alterations in DNA methylation and cold-responsive expression of *ACT1* are stably inherited and associated with acquired cold tolerance.

We used SunTag[29] to demethylate the hypermethylated region upstream of *ACT1* in KD8-4N. In two independent transgene-free lines, methylation levels were reduced to levels similar to KD8-4C (Figure 3A). *ACT1* expression remained unchanged in both lines upon cold stress, compared with downregulation in the negative-control line (Figure 3B), and seed set upon cold was increased (Figure 3C). Grain yield per plant increased with no obvious change in other agronomic traits (Figures S3A–S3D). Upon methylation restoration in KD8-4C, using a DNA-methylation editing system (Figure S3E), the resulting transgene-free lines

(F) Scatterplot showing the linear correlation between *ACT1* methylation (CG) and seed-setting ratio among the progenies from F_2 populations of KD8-4N and KD8-4C. Statistical significance is determined by Pearson's product-moment correlation. *R*, Pearson's correlation coefficient.
(G) DNA-methylation status in *ACT1* by Chop-PCR in higher generations of KD8-4C/4N inbred lines at normal temperature. 3N–5N indicates the generation numbers at normal temperature.
(H) *ACT1* expression in higher generations of KD8-4C/4N inbred lines at normal and cold temperatures. Relative expression was normalized to *UBIQUITIN* and values are means ± SD of three biological replicates. $^{**}p < 0.01$, Student's t test.
See also Figure S2 and Table S2.

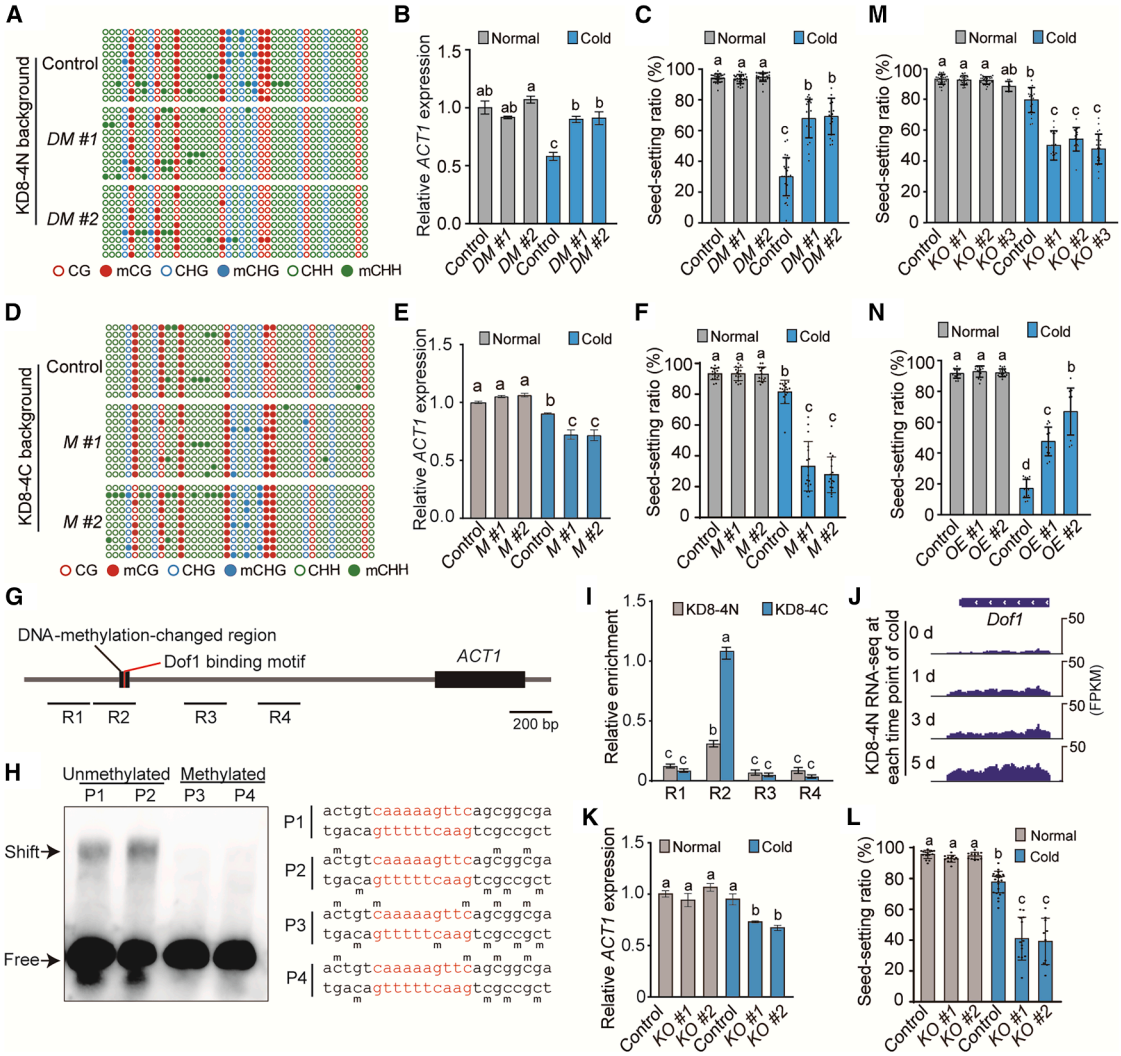

Figure 3. Targeted DNA demethylation of *ACT1* in KD8 enables cold-tolerance acquisition

(A) Bisulfite sequencing of the *ACT1* region in the negative control and two independent T_3 transgene-free lines for targeted demethylation of *ACT1* (*DM #1*, *DM #2*) in the KD8-4N background.

(B and C) *ACT1* expression in meiotic panicles (B) and seed-setting ratio (C) of negative control, *DM #1*, and *DM #2* lines at normal and cold temperatures. Statistically significant differences are indicated by different lowercase letters (B, ordinary two-way ANOVA with Tukey's multiple comparisons test, $p < 0.01$; C, Kruskal-Wallis test with Dunn's multiple comparisons test, $p < 0.01$).

(D) Bisulfite sequencing of the *ACT1* region in the negative control and two independent T_2 transgene-free lines for targeted methylation of *ACT1* (*M #1*, *M #2*) in the KD8-4C background.

(E and F) *ACT1* expression in meiotic panicles (E) and seed-setting ratio (F) of negative control, *M #1*, and *M #2* lines at normal and cold temperatures. Statistically significant differences are indicated by different lowercase letters (E, ordinary two-way ANOVA with Tukey's multiple comparisons test, $p < 0.01$; F, Kruskal-Wallis test with Dunn's multiple comparisons test, $p < 0.01$).

(G) Schematic of *ACT1* with the DNA-methylation-changed region and Dof1 binding site in the upstream sequence. Red vertical line denotes the Dof1 binding motif. Black lines indicate regions (R1–R4) detected by chromatin immunoprecipitation (ChIP)-qPCR.

(H) EMSA of MBP-Dof1 binding to the unmethylated probe sequence *in vitro*, with weaker affinity for probe sequences containing one or more methylated cytosines at the binding site.

(I) ChIP-qPCR assay of Dof1-FLAG binding to the *ACT1* promoter *in vivo*. Statistically significant differences are indicated by different lowercase letters, one-way ANOVA with Tukey's multiple comparisons test, $p < 0.01$.

(J) RNA-seq read coverage of *Dof1* in KD8-4N at the indicated cold-treatment time points. FPKM, fragments per kilobase per million.

(K and L) Relative *ACT1* expression in meiotic panicles (K) and seed-setting ratio (L) of negative control, *Dof1 KO #1*, and *KO #2* lines at normal and cold temperatures. Statistically significant differences are indicated by different lowercase letters (K, two-way ANOVA with Tukey's multiple comparisons test, $p < 0.01$; L, Kruskal-Wallis test with Dunn's multiple comparisons test, $p < 0.01$).

(legend continued on next page)

(*M #1*, *M #2*) displayed increased sensitivity to cold stress, with both *ACT1* expression and seed-setting ratio reduced upon cold treatment, compared with the negative control (Figures 3D–3F). DNA hypomethylation in the *ACT1* upstream region therefore accounts for its cold-insensitive expression and the increase in cold tolerance in plants bearing this epigenetic change.

Transcription factors regulate gene expression, and their target binding is influenced by DNA methylation.[30] The *ACT1* promoter contains a predicted binding motif (CAAAAAGTTCA) for the transcription factor Dof1.[31] This motif contains a cytosine (−1,519 CHG) subject to differential methylation (Figure 3G). In EMSAs, maltose binding protein (MBP)-Dof1 can bind unmethylated probes, while methylated probes containing methylated cytosine at position −1,519 weakened this (Figures 3H and S3F). Dof1-FLAG had a higher binding affinity to the *ACT1* promoter motif *in vivo* in the hypomethylated KD8-4C background, compared with the hypermethylated KD8-4N (Figure 3I).

Dof1 is itself cold-induced and activates transcription (Figures 3J and S3G). In *dof1* mutants (Figure S3H), *ACT1* expression was reduced under cold stress, and cold tolerance decreased (Figures 3K and 3L). Insensitivity of *ACT1* expression to cold stress in KD8-4C is therefore due to hypomethylation of its upstream region, which facilitates the binding of the cold-induced Dof1 and positively regulates its expression.

ACT1 hypomethylation underwent selection as a cold-adaptation target

ACT1 encodes ARABINOGALACTAN PROTEIN 1 (AGP1), which belongs to a family of extracellular glycoproteins implicated in plant growth, development, and environmental interactions.[32,33] To determine whether ACT1 functions in the cold response, we generated independent knockout and *ACT1-3xFLAG* overexpression lines in KD8-4C and KD8-4N backgrounds, respectively (Figures S3I–S3K). Upon cold stress, all three knockout lines had decreased cold-tolerance acquisition, whereas the *ACT1-3xFLAG* lines acquired cold tolerance, as inferred by seed set (Figures 3M and 3N). These results indicate that ACT1 function is required for cold tolerance during meiosis.

We analyzed *ACT1* minor-allele frequency of 2,847 sequenced accessions belonging to 9 subpopulations.[34] No high-frequency variation was seen across the *ACT1* region (2-kb promoter region + gene body + 1 kb downstream), with methylated nucleotides identical in all sampled accessions (Figure S3L).

We checked *ACT1* methylation status in the 31 varieties and landraces used to evaluate cold-tolerance acquisition (Table S1). Variation at the −1,549- to −1,513-bp region exists among them (Figure 4A), and methylation levels highly correlated with *ACT1* expression upon cold treatment (Pearson's $R = -0.801$, $p = 6.4e^{-8}$ for CG; $R = -0.809$, $p = 3.6e^{-8}$ for CHG; Figures 4B and S3M). Plants with hypermethylated DNA had weaker *ACT1* expression upon cold. A strong correlation exists for cold-tolerance acquisition with both *ACT1* methylation (Pearson's $R = -0.84$, $p = 3.5e^{-9}$ for CG; $R = -0.851$, $p = 1.4e^{-9}$ for CHG; Figures 4C and S3N) and its cold-induced differential expression (Pearson's $R = 0.928$, $p = 5.5e^{-14}$; Figure 4D). The accessions were further divided into cold-sensitive/tolerant groups based on a threshold of 50% seed set upon cold treatment. Similarly, *ACT1* epialleles were divided into low/high-methylation groups based on the threshold of the mean number of average mCG or mCHG in the −1,549- to −1,513-bp region between KD8-4N and KD8-4C. All nine cold-sensitive varieties bore high-methylation epialleles, while 95.4% (21/22) of cold-tolerant varieties had low-methylation *ACT1* epialleles (Figures 4C and S3N). DNA-methylation editing demethylated the hypermethylated *ACT1* in a cold-sensitive variety (CS1) and methylated hypomethylated *ACT1* in a cold-tolerant variety (CT19). These edited lines exhibited cold-insensitive *ACT1* expression and improved cold tolerance or exhibited cold-sensitive *ACT1* expression and were cold sensitive, respectively (Figures 4E–4J). Natural *ACT1* epialleles may therefore contribute to divergence in cold tolerance.

Crop landraces are sources of genetic or epigenetic variation associated with adaptations to diverse geographical regions.[35,36] Variation associated with adaptive cold tolerance during range expansion may be preserved in local landraces. We investigated methylation status at *ACT1* in 131 landraces from 3 major cropping regions across China, which span diverse geographic origins (Figure 4K; Table S3). Region 1 is located in southern coastal China, characterized by the highest annual active-accumulated temperature (AAT, $\geq 10^{\circ}C$), which is the main heat resource index for crop growth and development; region 2 is immediately north of and mostly inland of region 1 with a cooler but moderate AAT; and region 3 is located in northern China with the lowest AAT.[37] Methylation levels correlate strongly with geographic distribution, as determined by Chop-PCR (Figure 4K). In the southern regions, over 88% (31/35 in region 1; 63/71 in region 2) of the landraces have high DNA-methylation levels in *ACT1*. By contrast, the hypomethylation allele is highly enriched in region 3, from which 72% (18/25) have low methylation. Wild rice accessions[38] harbor hypermethylated *ACT1* epialleles (Figure S3O). These findings suggest that during the northward range expansion, *ACT1* hypomethylation was selected among landraces and may have contributed to cold adaptation.

Cold-induced downregulation of *MET1b* likely contributes to hypomethylated *ACT1* epiallele formation

We next explored how cold could induce the *ACT1* hypomethylation epiallele. Of the 10 DNA methyltransferases and 5 demethylases encoded in the rice genome,[39,40] *DNA METHYLTRANSFERASE 1b* (*MET1b*) and *CHROMOMETHYLASE 3* (*CMT3*) were downregulated in meiotic panicles upon cold treatment in KD8-4N and in other varieties (Figures 4A, S4A, and S4B). To determine whether and to what extent cold-induced downregulation of both methyltransferases are responsible for the formation of hypomethylation epialleles, we generated

(M and N) Seed-setting ratio of negative control, three *act1* knockout mutants (M) and two transgenic *ACT1* overexpression lines (*OE #1*, *OE #2*) (N) at normal and cold temperatures. Statistically significant differences are indicated by different lowercase letters (Kruskal-Wallis test with Dunn's multiple comparisons test, $p < 0.01$).
See also Figure S3.

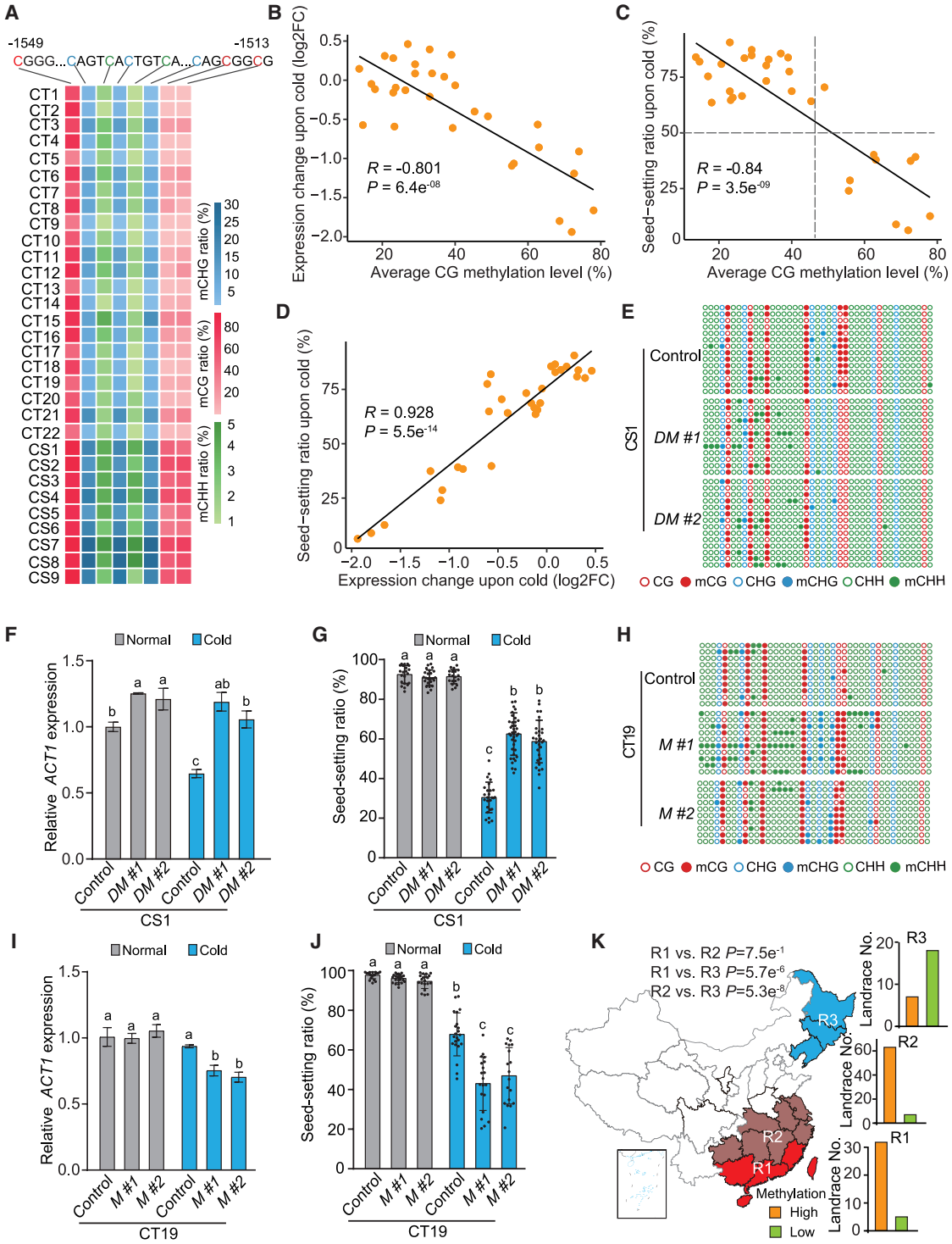

Figure 4. Natural variation in *ACT1* methylation correlates with cold tolerance and latitudinal distribution of rice accessions

(A) DNA-methylation status of the *ACT1* upstream region in 31 varieties/landraces from northern China. The methylated cytosine ratio was determined by bisulfite sequencing.

(B–D) Correlations between DNA-methylation level (CG) and *ACT1* expression changes upon cold (B), *ACT1* DNA-methylation level (CG) and seed-setting ratio (C), and *ACT1* expression changes upon cold and seed-setting ratio (D) in 31 varieties/landraces. The dashed lines in (C) indicate the thresholds of cold-sensitive/tolerant groups or low/high DNA-methylation groups. Statistical significance of correlations was determined by Pearson's product-moment correlation. *R*, Pearson correlation coefficient.

(legend continued on next page)

RNAi lines against *MET1b* and *CMT3* in the KD8-4N background (Figure S4C) and performed bisulfite sequencing. *ACT1* represents a typical MET1b-dependent DMR. Both *MET1b* RNAi lines exhibit the same DNA-methylation variation at the *ACT1* locus as observed in KD8-4C by cold induction, affecting identical sites and to almost the same extent: three CG and three CHG sites spanning a 37-bp region at −1,549 to −1,513 bp, which show hypomethylation in *MET1b* RNAi lines (Figure S4D).

The stable formation of hypomethylated epialleles also requires the absence of *de novo* DNA methylation, which is typically directed by 24-nt small interfering RNAs (siRNAs) in plants.[28] Small RNA sequencing (RNA-seq) revealed no detectable 24-nt siRNAs targeting the region near the methylation variation sites at *ACT1* in KD8-4N and KD8-4C under normal and cold conditions (Figure S4D).

This finding suggests that the upstream CG methylation sites of *ACT1* are directly regulated by MET1b, implying that the cold-induced downregulation of *MET1b* likely mediates the formation of epi-*ACT1*. Methylation at this locus is easily lost when there is a disruption therein and in the absence of small RNA(s) targeting the vicinity of the locus.

DISCUSSION

Epigenetic marks can rapidly be changed in response to environmental changes, and plants and animals can experience heritable epigenetic variation due to environmental stimuli. This has prompted calls to include these mechanisms in contemporary evolutionary theory.[41] However, the adaptive significance and long-term stability of such changes are debated because specific causal loci for stably inherited adaptive traits from epigenetic variation have not been clearly identified.[5]

Here, we demonstrate that a heritable epigenetic change in *ACT1* that confers cold tolerance can be acquired through low-temperature treatment of rice. This environmentally directed epigenetic variation is stably inherited without continuous environmental stimuli, likely aiding northward expansion of rice. We offer evidence supporting the notion that environment-directed epigenetic changes to phenotypic variation can serve as natural selection targets, suggesting a need to rethink evolutionary theory.

The evolutionary significance of these environmentally directed epimutations lies in their potential to provide immediate adaptive benefits, such as enhancing survival and fitness. Moreover, such environmentally directed epigenetic changes may become fixed within populations, contributing to long-term evolutionary processes. For example, at the *ACT1* locus, there is natural variation in DNA-methylation status, with hypomethylated alleles enriched in cold-tolerant rice in a cold cropping region in China.

Our results also inform a possible means through how the environment directs the formation of epialleles, at least from cold treatment to rice at booting stage when temperature-sensitive meiosis is occurring. We propose that during rice's northward expansion, cold-induced epigenetic variations arise when low temperatures during the meiotic stage downregulate *MET1b* and *CMT3*, resulting in a failure to reinforce DNA methylation in CG/CHG contexts at certain loci.[42] Exposure of successive generations to low temperatures strengthens and stabilizes the loss of methylation, creating stable epialleles that help rice adapt to colder climates (Figure S4E). The *ACT1* epiallele exemplifies this process by promoting high *AGP1* expression during cold stress, which is crucial for cold tolerance. Its arabinogalactan protein product is subject to GPI lipid anchoring, allowing it to bind to the plasma membrane. By binding calcium ions, it forms an AGP-Ca^{2+} capacitor,[43] likely playing a role in sensing and transmitting cold signals, thereby mediating cold tolerance.

Limitations of the study

A key point for future investigation is the generality of cold-induced epialleles in mediating acquired cold tolerance by conducting acclimation experiments with more cold-sensitive accessions. However, the current method cannot ensure that all florets are at the cold-sensitive meiotic stage during cold treatment, leading to uncertainty in the initial screening and limiting its large-scale application. To overcome this, non-destructive tools for efficiently detecting, labeling, and tracking young florets are needed. This would enable high-throughput phenotypic screening, precise sampling, and omics analysis of specific cells to identify causal variant loci.

Although we have genetically confirmed that *ACT1* plays a critical role in cold tolerance at booting, the mechanisms by which methylation regulates *ACT1* expression in response to cold stress, as well as how ACT1 controls pollen development at low temperatures, require investigation.

RESOURCE AVAILABILITY

Lead contact

Further information and requests for resources and reagents should be directed to and will be fulfilled by the lead contact, Xiaofeng Cao (xfcao@genetics.ac.cn).

(E) Bisulfite sequencing of the *ACT1* region in the negative control and two independent T_3 transgene-free lines for targeted demethylation of *ACT1* (*DM #1*, *DM #2*) in variety CS1.

(F and G) *ACT1* expression in meiotic panicles (F) and seed-setting ratio (G) of negative control, *DM #1*, and *DM #2* lines in variety CS1 at normal and cold temperatures. Statistically significant differences are indicated by different lowercase letters (F, two-way ANOVA with Tukey's multiple comparisons test, $p < 0.01$; G, Kruskal-Wallis test with Dunn's multiple comparisons test, $p < 0.01$).

(H) Bisulfite sequencing of the *ACT1* region in the negative control and two independent T_2 transgene-free lines for targeted methylation of *ACT1* (*M #1*, *M #2*) in variety CT19.

(I and J) Relative *ACT1* expression in meiotic panicles (I) and seed-setting ratio (J) of the negative control, *M #1*, and *M #2* lines in rice variety CT19 at normal and cold temperatures. Statistically significant differences are indicated by different lowercase letters (I, two-way ANOVA with Tukey's multiple comparisons test, $p < 0.01$; J, Kruskal-Wallis test with Dunn's multiple comparisons test, $p < 0.01$).

(K) Geographic distribution of landraces with differing DNA-methylation status at *ACT1* from three major cropping regions in China, designated regions 1–3 (R1: South China region, R2: Central China region, R3: Northeast China region). *p* values are determined by Student's t test.

See also Figures S3 and S4 and Tables S1 and S3.

Materials availability

Constructs, seeds, and unique reagents generated in this study will be available from the lead contact upon request with a completed materials transfer agreement.

Data and code availability

The RNA-seq, whole-genome bisulfite sequencing (WGBS), and whole-genome sequencing data generated in this study are publicly accessible through the Genome Sequence Archive (GSA: https://ngdc.cncb.ac.cn/gsa/) at the Beijing Institute of Genomics, Chinese Academy of Sciences, under accession number PRJCA016978. Genome assemblies and annotation files are available via the Science Data Bank at https://doi.org/10.57760/sciencedb.08245. Additional data supporting the findings of this study can be obtained from the corresponding author upon reasonable request.

ACKNOWLEDGMENTS

We thank Wen Wang (Northwestern Polytechnical University) and Falong Lu (Institute of Genetics and Developmental Biology, Chinese Academy of Sciences) for their critical reading and suggestions. We thank Guy Riddihough for the help with editing the manuscript. We thank the National Mid-term GenBank for Rice of China National Rice Research Institute for providing the landraces. We thank Ge Song (Institute of Botany, Chinese Academy of Sciences) for providing the wild rice accessions.

This work was supported by the National Key R&D Program of China (2023ZD04073 to X.C.), the National Natural Science Foundation of China (32330019 to X.C., 32170620 to X.S., and 32101654 to X.-L.H.), the Strategic Priority Research Program of the Chinese Academy of Sciences (XDA28030100 to X.S), the National Key Research and Development Program (2020YFA0509903 to X.C. and 2022YFF1002802 to X.D.), The Major Program for Basic Research Project of Yunnan Province (202401BC070001 to H. Liu), the Yunnan Revitalization Talent Support Program "Young Talent" project (XDYC-QNRC-2022-0423 to H. Liu), the Youth Innovation Promotion Association of CAS (Y2022039 to X.D.), and the Postdoctoral Fellowship Program (Grade B) of China Postdoctoral Science Foundation (GZB20240817 to S.T.).

AUTHOR CONTRIBUTIONS

X.S. and X.C. designed the study and wrote the manuscript; X.S., S.T., Y.M., Z. G., X.-L.H., L.W., B.Y., X.D., and S.J. performed the experiments; and H. Liu, H. Luo, B.W., and C.Y. analyzed the data.

DECLARATION OF INTERESTS

The authors declare no competing interests.

STAR★METHODS

Detailed methods are provided in the online version of this paper and include the following:

- KEY RESOURCES TABLE
- EXPERIMENTAL MODEL AND STUDY PARTICIPANT DETAILS
  - Plant materials and growth conditions
- METHOD DETAILS
  - Plant cold treatment
  - Generation of transgenic rice plants
  - Total RNA isolation and qRT–PCR analysis
  - PCR amplification with methylation-sensitive restriction enzyme (Chop–PCR)
  - Bisulfite-sequencing-based DNA-methylation analysis
  - EMSA
  - ChIP–qPCR assay
  - Transcriptional activity assay
  - Genome sequencing, assembly and annotation
  - Identification of variation between KD8-4C and KD8-4N genomes
  - Transcriptome analysis
  - Whole-genome bisulfite-sequencing data processing
  - Identification of differentially methylated regions
  - Characterization of the *ACT1* locus
  - Small-RNA analysis
- QUANTIFICATION AND STATISTICAL ANALYSIS

SUPPLEMENTAL INFORMATION

Supplemental information can be found online at https://doi.org/10.1016/j.cell.2025.04.036.

Received: September 17, 2024
Revised: December 28, 2024
Accepted: April 27, 2025
Published: May 22, 2025

REFERENCES

1. Loison, L. (2018). Lamarckism and epigenetic inheritance: a clarification. Biol. Philos. *33*, 29. https://doi.org/10.1007/s10539-018-9642-2.
2. Durrant, A. (1958). Environmental conditioning of flax. Nature *181*, 928–929. https://doi.org/10.1038/181928a0.
3. Pawlow, I.P. (1923). New researches on conditioned reflexes. Science *58*, 359–361. https://doi.org/10.1126/science.58.1506.359.
4. Gorczynski, R.M., and Steele, E.J. (1981). Simultaneous yet independent inheritance of somatically acquired tolerance to two distinct H-2 antigenic haplotype determinants in mice. Nature *289*, 678–681. https://doi.org/10.1038/289678a0.
5. Laland, K., Uller, T., Feldman, M., Sterelny, K., Müller, G.B., Moczek, A., Jablonka, E., Odling-Smee, J., Wray, G.A., Hoekstra, H.E., et al. (2014). Does evolutionary theory need a rethink? Nature *514*, 161–164. https://doi.org/10.1038/514161a.
6. Rechavi, O., Houri-Ze'evi, L., Anava, S., Goh, W.S.S., Kerk, S.Y., Hannon, G.J., and Hobert, O. (2014). Starvation-induced transgenerational inheritance of small RNAs in *C. elegans*. Cell *158*, 277–287. https://doi.org/10.1016/j.cell.2014.06.020.
7. Dubin, M.J., Zhang, P., Meng, D., Remigereau, M.S., Osborne, E.J., Paolo Casale, F., Drewe, P., Kahles, A., Jean, G., Vilhjálmsson, B., et al. (2015). DNA methylation in Arabidopsis has a genetic basis and shows evidence of local adaptation. eLife *4*, e05255. https://doi.org/10.7554/eLife.05255.
8. Wibowo, A., Becker, C., Marconi, G., Durr, J., Price, J., Hagmann, J., Papareddy, R., Putra, H., Kageyama, J., Becker, J., et al. (2016). Hyperosmotic stress memory in Arabidopsis is mediated by distinct epigenetically labile sites in the genome and is restricted in the male germline by DNA glycosylase activity. eLife *5*, e13546. https://doi.org/10.7554/eLife.13546.
9. Zhang, Y., Zhang, X., Shi, J., Tuorto, F., Li, X., Liu, Y., Liebers, R., Zhang, L., Qu, Y., Qian, J., et al. (2018). Dnmt2 mediates intergenerational transmission of paternally acquired metabolic disorders through sperm small non-coding RNAs. Nat. Cell Biol. *20*, 535–540. https://doi.org/10.1038/s41556-018-0087-2.
10. Dias, B.G., and Ressler, K.J. (2014). Parental olfactory experience influences behavior and neural structure in subsequent generations. Nat. Neurosci. *17*, 89–96. https://doi.org/10.1038/nn.3594.
11. Chen, Q., Yan, M., Cao, Z., Li, X., Zhang, Y., Shi, J., Feng, G.H., Peng, H., Zhang, X., Zhang, Y., et al. (2016). Sperm tsRNAs contribute to intergenerational inheritance of an acquired metabolic disorder. Science *351*, 397–400. https://doi.org/10.1126/science.aad7977.
12. Radford, E.J., Ito, M., Shi, H., Corish, J.A., Yamazawa, K., Isganaitis, E., Seisenberger, S., Hore, T.A., Reik, W., Erkek, S., et al. (2014). In utero effects. In utero undernourishment perturbs the adult sperm methylome and intergenerational metabolism. Science *345*, 1255903. https://doi.org/10.1126/science.1255903.
13. Fitz-James, M.H., and Cavalli, G. (2022). Molecular mechanisms of transgenerational epigenetic inheritance. Nat. Rev. Genet. *23*, 325–341. https://doi.org/10.1038/s41576-021-00438-5.

14. Soppe, W.J.J., Jacobsen, S.E., Alonso-Blanco, C., Jackson, J.P., Kakutani, T., Koornneef, M., and Peeters, A.J.M. (2000). The late flowering phenotype of fwa mutants is caused by gain-of-function epigenetic alleles of a homeodomain gene. Mol. Cell *6*, 791–802. https://doi.org/10.1016/s1097-2765(05)00090-0.

15. Cubas, P., Vincent, C., and Coen, E. (1999). An epigenetic mutation responsible for natural variation in floral symmetry. Nature *401*, 157–161. https://doi.org/10.1038/43657.

16. Manning, K., Tör, M., Poole, M., Hong, Y., Thompson, A.J., King, G.J., Giovannoni, J.J., and Seymour, G.B. (2006). A naturally occurring epigenetic mutation in a gene encoding an SBP-box transcription factor inhibits tomato fruit ripening. Nat. Genet. *38*, 948–952. https://doi.org/10.1038/ng1841.

17. Jacobsen, S.E., and Meyerowitz, E.M. (1997). Hypermethylated SUPERMAN epigenetic alleles in arabidopsis. Science *277*, 1100–1103. https://doi.org/10.1126/science.277.5329.1100.

18. Martin, A., Troadec, C., Boualem, A., Rajab, M., Fernandez, R., Morin, H., Pitrat, M., Dogimont, C., and Bendahmane, A. (2009). A transposon-induced epigenetic change leads to sex determination in melon. Nature *461*, 1135–1138. https://doi.org/10.1038/nature08498.

19. Zhang, L., Yu, H., Ma, B., Liu, G., Wang, J., Wang, J., Gao, R., Li, J., Liu, J., Xu, J., et al. (2017). A natural tandem array alleviates epigenetic repression of IPA1 and leads to superior yielding rice. Nat. Commun. *8*, 14789. https://doi.org/10.1038/ncomms14789.

20. Ma, Y., Dai, X., Xu, Y., Luo, W., Zheng, X., Zeng, D., Pan, Y., Lin, X., Liu, H., Zhang, D., et al. (2015). COLD1 confers chilling tolerance in rice. Cell *160*, 1209–1221. https://doi.org/10.1016/j.cell.2015.01.046.

21. Huang, X., Kurata, N., Wei, X., Wang, Z.X., Wang, A., Zhao, Q., Zhao, Y., Liu, K., Lu, H., Li, W., et al. (2012). A map of rice genome variation reveals the origin of cultivated rice. Nature *490*, 497–501. https://doi.org/10.1038/nature11532.

22. Gutaker, R.M., Groen, S.C., Bellis, E.S., Choi, J.Y., Pires, I.S., Bocinsky, R.K., Slayton, E.R., Wilkins, O., Castillo, C.C., Negrão, S., et al. (2020). Genomic history and ecology of the geographic spread of rice. Nat. Plants *6*, 492–502. https://doi.org/10.1038/s41477-020-0659-6.

23. Hayase, H., Satake, T., Nishiyama, I., and Ito, N. (1969). Male Sterility Caused by Cooling Treatment at the Meiotic Stage in Rice Plants: II. The most sensitive stage to cooling and the fertilizing ability of pistils. Jpn. J. Crop Sci. *38*, 706–711. https://doi.org/10.1626/jcs.38.706.

24. Chen, R., Deng, Y., Ding, Y., Guo, J., Qiu, J., Wang, B., Wang, C., Xie, Y., Zhang, Z., Chen, J., et al. (2022). Rice functional genomics: decades' efforts and roads ahead. Sci. China Life Sci. *65*, 33–92. https://doi.org/10.1007/s11427-021-2024-0.

25. Li, J., Zhang, Z., Chong, K., and Xu, Y. (2022). Chilling tolerance in rice: Past and present. J. Plant Physiol. *268*, 153576. https://doi.org/10.1016/j.jplph.2021.153576.

26. Zhang, Z., Li, J., Pan, Y., Li, J., Zhou, L., Shi, H., Zeng, Y., Guo, H., Yang, S., Zheng, W., et al. (2017). Natural variation in CTB4a enhances rice adaptation to cold habitats. Nat. Commun. *8*, 14788. https://doi.org/10.1038/ncomms14788.

27. Kuroki, M., Saito, K., Matsuba, S., Yokogami, N., Shimizu, H., Ando, I., and Sato, Y. (2007). A quantitative trait locus for cold tolerance at the booting stage on rice chromosome 8. Theor. Appl. Genet. *115*, 593–600. https://doi.org/10.1007/s00122-007-0589-y.

28. Lloyd, J.P.B., and Lister, R. (2022). Epigenome plasticity in plants. Nat. Rev. Genet. *23*, 55–68. https://doi.org/10.1038/s41576-021-00407-y.

29. Tang, S., Yang, C., Wang, D., Deng, X., Cao, X., and Song, X. (2022). Targeted DNA demethylation produces heritable epialleles in rice. Sci. China Life Sci. *65*, 753–756. https://doi.org/10.1007/s11427-021-1974-7.

30. O'Malley, R.C., Huang, S.C., Song, L., Lewsey, M.G., Bartlett, A., Nery, J.R., Galli, M., Gallavotti, A., and Ecker, J.R. (2016). Cistrome and Epicistrome Features Shape the Regulatory DNA Landscape. Cell *165*, 1280–1292. https://doi.org/10.1016/j.cell.2016.04.038.

31. Lijavetzky, D., Carbonero, P., and Vicente-Carbajosa, J. (2003). Genome-wide comparative phylogenetic analysis of the rice and Arabidopsis Dof gene families. BMC Evol. Biol. *3*, 17. https://doi.org/10.1186/1471-2148-3-17.

32. Seifert, G.J., and Roberts, K. (2007). The biology of arabinogalactan proteins. Annu. Rev. Plant Biol. *58*, 137–161. https://doi.org/10.1146/annurev.arplant.58.032806.103801.

33. Delmer, D., Dixon, R.A., Keegstra, K., and Mohnen, D. (2024). The plant cell wall-dynamic, strong, and adaptable-is a natural shapeshifter. Plant Cell *36*, 1257–1311. https://doi.org/10.1093/plcell/koad325.

34. Wang, W., Mauleon, R., Hu, Z., Chebotarov, D., Tai, S., Wu, Z., Li, M., Zheng, T., Fuentes, R.R., Zhang, F., et al. (2018). Genomic variation in 3,010 diverse accessions of Asian cultivated rice. Nature *557*, 43–49. https://doi.org/10.1038/s41586-018-0063-9.

35. Mercer, K.L., and Perales, H.R. (2010). Evolutionary response of landraces to climate change in centers of crop diversity. Evol. Appl. *3*, 480–493. https://doi.org/10.1111/j.1752-4571.2010.00137.x.

36. Ramirez-Villegas, J., Khoury, C.K., Achicanoy, H.A., Diaz, M.V., Mendez, A.C., Sosa, C.C., Kehel, Z., Guarino, L., Abberton, M., Aunario, J., et al. (2022). State of ex situ conservation of landrace groups of 25 major crops. Nat. Plants *8*, 491–499. https://doi.org/10.1038/s41477-022-01144-8.

37. Mei, F., Wu, X., Yao, C., Li, L., Wang, L., and Chen, Q. (1988). Rice Cropping Regionalization in China. Chin. J. Rice Sci. *2*, 97–110.

38. Jing, C.Y., Zhang, F.M., Wang, X.H., Wang, M.X., Zhou, L., Cai, Z., Han, J.D., Geng, M.F., Yu, W.H., Jiao, Z.H., et al. (2023). Multiple domestications of Asian rice. Nat. Plants *9*, 1221–1235. https://doi.org/10.1038/s41477-023-01476-z.

39. Sharma, R., Mohan Singh, R.K., Malik, G., Deveshwar, P., Tyagi, A.K., Kapoor, S., and Kapoor, M. (2009). Rice cytosine DNA methyltransferases - gene expression profiling during reproductive development and abiotic stress. FEBS J. *276*, 6301–6311. https://doi.org/10.1111/j.1742-4658.2009.07338.x.

40. La, H., Ding, B., Mishra, G.P., Zhou, B., Yang, H., Bellizzi, R., Chen, S., Meyers, B.C., Peng, Z., Zhu, J.K., et al. (2011). A 5-methylcytosine DNA glycosylase/lyase demethylates the retrotransposon Tos17 and promotes its transposition in rice. Proc. Natl. Acad. Sci. USA *108*, 15498–15503. https://doi.org/10.1073/pnas.1112704108.

41. Skinner, M.K. (2015). Environmental Epigenetics and a Unified Theory of the Molecular Aspects of Evolution: A Neo-Lamarckian Concept that Facilitates Neo-Darwinian Evolution. Genome Biol. Evol. *7*, 1296–1302. https://doi.org/10.1093/gbe/evv073.

42. Quadrana, L., and Colot, V. (2016). Plant Transgenerational Epigenetics. Annu. Rev. Genet. *50*, 467–491. https://doi.org/10.1146/annurev-genet-120215-035254.

43. Lopez-Hernandez, F., Tryfona, T., Rizza, A., Yu, X.L.L., Harris, M.O.B., Webb, A.A.R., Kotake, T., and Dupree, P. (2020). Calcium Binding by Arabinogalactan Polysaccharides Is Important for Normal Plant Development. Plant Cell *32*, 3346–3369. https://doi.org/10.1105/tpc.20.00027.

44. Wang, K., Wang, J., Zhu, C., Yang, L., Ren, Y., Ruan, J., Fan, G., Hu, J., Xu, W., Bi, X., et al. (2021). African lungfish genome sheds light on the vertebrate water-to-land transition. Cell *184*, 1362–1376.e18. https://doi.org/10.1016/j.cell.2021.01.047.

45. Li, H. (2018). Minimap2: pairwise alignment for nucleotide sequences. Bioinformatics *34*, 3094–3100. https://doi.org/10.1093/bioinformatics/bty191.

46. Bolger, A.M., Lohse, M., and Usadel, B. (2014). Trimmomatic: a flexible trimmer for Illumina sequence data. Bioinformatics *30*, 2114–2120. https://doi.org/10.1093/bioinformatics/btu170.

47. Hu, J., Fan, J., Sun, Z., and Liu, S. (2020). NextPolish: a fast and efficient genome polishing tool for long-read assembly. Bioinformatics *36*, 2253–2255. https://doi.org/10.1093/bioinformatics/btz891.

48. Alonge, M., Soyk, S., Ramakrishnan, S., Wang, X.G., Goodwin, S., Sedlazeck, F.J., Lippman, Z.B., and Schatz, M.C. (2019). RaGOO: fast and

accurate reference-guided scaffolding of draft genomes. Genome Biol. *20*, 224. https://doi.org/10.1186/s13059-019-1829-6.

49. Manni, M., Berkeley, M.R., Seppey, M., Simão, F.A., and Zdobnov, E.M. (2021). BUSCO Update: Novel and Streamlined Workflows along with Broader and Deeper Phylogenetic Coverage for Scoring of Eukaryotic, Prokaryotic, and Viral Genomes. Mol. Biol. Evol. *38*, 4647–4654. https://doi.org/10.1093/molbev/msab199.
50. Smit, A., Hubley, R., and Green, P. (2013–2015). RepeatMasker Open-4.0. http://www.repeatmasker.org.
51. Smit, A., and Hubley, R. (2008–2015). RepeatModeler Open-1.0. http://www.repeatmasker.org.
52. Ou, S., Su, W., Liao, Y., Chougule, K., Agda, J.R.A., Hellinga, A.J., Lugo, C.S.B., Elliott, T.A., Ware, D., Peterson, T., et al. (2019). Benchmarking transposable element annotation methods for creation of a streamlined, comprehensive pipeline. Genome Biol. *20*, 275. https://doi.org/10.1186/s13059-019-1905-y.
53. Campbell, M.S., Holt, C., Moore, B., and Yandell, M. (2014). Genome Annotation and Curation Using MAKER and MAKER-P. Curr. Protoc. Bioinformatics *48*, 4.11.1–4.11.39. https://doi.org/10.1002/0471250953.bi0411s48.
54. Kim, D., Paggi, J.M., Park, C., Bennett, C., and Salzberg, S.L. (2019). Graph-based genome alignment and genotyping with HISAT2 and HISAT-genotype. Nat. Biotechnol. *37*, 907–915. https://doi.org/10.1038/s41587-019-0201-4.
55. Korf, I. (2004). Gene finding in novel genomes. BMC Bioinform. *5*, 59. https://doi.org/10.1186/1471-2105-5-59.
56. Goel, M., Sun, H., Jiao, W.B., and Schneeberger, K. (2019). SyRI: finding genomic rearrangements and local sequence differences from whole-genome assemblies. Genome Biol. *20*, 277. https://doi.org/10.1186/s13059-019-1911-0.
57. Li, H., and Durbin, R. (2009). Fast and accurate short read alignment with Burrows-Wheeler transform. Bioinformatics *25*, 1754–1760. https://doi.org/10.1093/bioinformatics/btp324.
58. McKenna, A., Hanna, M., Banks, E., Sivachenko, A., Cibulskis, K., Kernytsky, A., Garimella, K., Altshuler, D., Gabriel, S., Daly, M., et al. (2010). The Genome Analysis Toolkit: a MapReduce framework for analyzing next-generation DNA sequencing data. Genome Res. *20*, 1297–1303. https://doi.org/10.1101/gr.107524.110.
59. Quinlan, A.R., and Hall, I.M. (2010). BEDTools: a flexible suite of utilities for comparing genomic features. Bioinformatics *26*, 841–842. https://doi.org/10.1093/bioinformatics/btq033.
60. Kovaka, S., Zimin, A.V., Pertea, G.M., Razaghi, R., Salzberg, S.L., and Pertea, M. (2019). Transcriptome assembly from long-read RNA-seq alignments with StringTie2. Genome Biol. *20*, 278. https://doi.org/10.1186/s13059-019-1910-1.
61. Leek, J.T., Johnson, W.E., Parker, H.S., Jaffe, A.E., and Storey, J.D. (2012). The sva package for removing batch effects and other unwanted variation in high-throughput experiments. Bioinformatics *28*, 882–883. https://doi.org/10.1093/bioinformatics/bts034.
62. Kolde, R. (2018). pheatmap: Pretty Heatmaps. https://github.com/raivokolde/pheatmap.
63. Hadley, W. (2016). ggplot2: Elegant Graphics for Data Analysis (Springer-Verlag).
64. Love, M.I., Huber, W., and Anders, S. (2014). Moderated estimation of fold change and dispersion for RNA-seq data with DESeq2. Genome Biol. *15*, 550. https://doi.org/10.1186/s13059-014-0550-8.
65. Krueger, F., and Andrews, S.R. (2011). Bismark: a flexible aligner and methylation caller for Bisulfite-Seq applications. Bioinformatics *27*, 1571–1572. https://doi.org/10.1093/bioinformatics/btr167.
66. Akalin, A., Kormaksson, M., Li, S., Garrett-Bakelman, F.E., Figueroa, M.E., Melnick, A., and Mason, C.E. (2012). methylKit: a comprehensive R package for the analysis of genome-wide DNA methylation profiles. Genome Biol. *13*, R87. https://doi.org/10.1186/gb-2012-13-10-r87.
67. Langmead, B., and Salzberg, S.L. (2012). Fast gapped-read alignment with Bowtie 2. Nat. Methods *9*, 357–359. https://doi.org/10.1038/nmeth.1923.
68. Axtell, M.J. (2013). ShortStack: comprehensive annotation and quantification of small RNA genes. RNA *19*, 740–751. https://doi.org/10.1261/rna.035279.112.
69. Si, F.Y., Luo, H.F., Yang, C., Gong, J., Yan, B., Liu, C.Y., Song, X.W., and Cao, X.F. (2023). Mobile ARGONAUTE 1d binds 22-nt miRNAs to generate phasiRNAs important for low-temperature male fertility in rice. Sci. China Life Sci. *66*, 197–208. https://doi.org/10.1007/s11427-022-2204-y.
70. Zhang, T., Gao, Y., Wang, R., and Zhao, Y. (2017). Production of Guide RNAs in vitro and in vivo for CRISPR Using Ribozymes and RNA Polymerase II Promoters. Bio Protoc. *7*, e2148. https://doi.org/10.21769/BioProtoc.2148.
71. Ma, X., Zhang, Q., Zhu, Q., Liu, W., Chen, Y., Qiu, R., Wang, B., Yang, Z., Li, H., Lin, Y., et al. (2015). A Robust CRISPR/Cas9 System for Convenient, High-Efficiency Multiplex Genome Editing in Monocot and Dicot Plants. Mol. Plant *8*, 1274–1284. https://doi.org/10.1016/j.molp.2015.04.007.
72. Liu, B., Li, P., Li, X., Liu, C., Cao, S., Chu, C., and Cao, X. (2005). Loss of function of OsDCL1 affects microRNA accumulation and causes developmental defects in rice. Plant Physiol. *139*, 296–305. https://doi.org/10.1104/pp.105.063420.
73. Hiei, Y., Ohta, S., Komari, T., and Kumashiro, T. (1994). Efficient transformation of rice (Oryza sativa L.) mediated by Agrobacterium and sequence analysis of the boundaries of the T-DNA. Plant J. *6*, 271–282. https://doi.org/10.1046/j.1365-313x.1994.6020271.x.
74. Gruntman, E., Qi, Y.J., Slotkin, R.K., Roeder, T., Martienssen, R.A., and Sachidanandam, R. (2008). Kismeth: Analyzer of plant methylation states through bisulfite sequencing. BMC Bioinform. *9*, 371. https://doi.org/10.1186/1471-2105-9-371.
75. Sun, T., Liu, Q., Chen, X., Hu, F., and Wang, K. (2024). Hi-TOM 2.0: an improved platform for high-throughput mutation detection. Sci. China Life Sci. *67*, 1532–1534. https://doi.org/10.1007/s11427-024-2555-x.
76. Si, F., Yang, C., Yan, B., Yan, W., Tang, S., Yan, Y., Cao, X., and Song, X. (2022). Control of OsARF3a by OsKANADI1 contributes to lemma development in rice. Plant J. *110*, 1717–1730. https://doi.org/10.1111/tpj.15766.
77. Liu, W., Li, J., Sun, J., Liu, C., Yan, B., Zhou, C., Li, S., Song, X., Yan, W., Yang, Y., et al. (2025). The E3 ligase OsHel2 impedes readthrough of stalled mRNAs to regulate male fertility in thermosensitive genic male sterile rice. Plant Commun. *6*, 101192. https://doi.org/10.1016/j.xplc.2024.101192.
78. Tarailo-Graovac, M., and Chen, N. (2009). Using RepeatMasker to Identify Repetitive Elements in Genomic Sequences. Curr Protoc Bioinformatics *Chapter 4*, 4.10.1–4.10.14.
79. Stein, J.C., Yu, Y., Copetti, D., Zwickl, D.J., Zhang, L., Zhang, C., Chougule, K., Gao, D., Iwata, A., Goicoechea, J.L., et al. (2018). Genomes of 13 domesticated and wild rice relatives highlight genetic conservation, turnover and innovation across the genus Oryza. Nat. Genet. *50*, 285–296. https://doi.org/10.1038/s41588-018-0040-0.
80. Sakai, H., Lee, S.S., Tanaka, T., Numa, H., Kim, J., Kawahara, Y., Wakimoto, H., Yang, C.C., Iwamoto, M., Abe, T., et al. (2013). Rice Annotation Project Database (RAP-DB): an integrative and interactive database for rice genomics. Plant Cell Physiol. *54*, e6. https://doi.org/10.1093/pcp/pcs183.
81. Jiao, Y., Peluso, P., Shi, J., Liang, T., Stitzer, M.C., Wang, B., Campbell, M.S., Stein, J.C., Wei, X., Chin, C.S., et al. (2017). Improved maize reference genome with single-molecule technologies. Nature *546*, 524–527. https://doi.org/10.1038/nature22971.
82. Lamesch, P., Berardini, T.Z., Li, D., Swarbreck, D., Wilks, C., Sasidharan, R., Muller, R., Dreher, K., Alexander, D.L., Garcia-Hernandez, M., et al. (2012). The Arabidopsis Information Resource (TAIR): improved gene

annotation and new tools. Nucleic Acids Res. *40*, D1202–D1210. https://doi.org/10.1093/nar/gkr1090.

83. Kawahara, Y., de la Bastide, M., Hamilton, J.P., Kanamori, H., McCombie, W.R., Ouyang, S., Schwartz, D.C., Tanaka, T., Wu, J., Zhou, S., et al. (2013). Improvement of the Oryza sativa Nipponbare reference genome using next generation sequence and optical map data. Rice (N Y) *6*, 4. https://doi.org/10.1186/1939-8433-6-4.

84. Thorvaldsdóttir, H., Robinson, J.T., and Mesirov, J.P. (2013). Integrative Genomics Viewer (IGV): high-performance genomics data visualization and exploration. Brief. Bioinform. *14*, 178–192. https://doi.org/10.1093/bib/bbs017.

85. Langmead, B., Trapnell, C., Pop, M., and Salzberg, S.L. (2009). Ultrafast and memory-efficient alignment of short DNA sequences to the human genome. Genome Biol. *10*, R25. https://doi.org/10.1186/gb-2009-10-3-r25.

STAR★METHODS

KEY RESOURCES TABLE

REAGENT or RESOURCE	SOURCE	IDENTIFIER
Antibodies		
Rabbit monoclonal anti-DDDDK-Tag	Abclonal	Cat# AE092; RRID: AB_2940847
Bacterial and virus strains		
Agrobacterium tumefaciens EHA105	This study	N/A
Escherichia coli chemically competent cell DH5α	This study	N/A
Chemicals, peptides, and recombinant proteins		
*Pme*I	NEB	Cat# R0560V
*Aci*I	NEB	Cat# R0551V
TRIzol reagent	Invitrogen	Cat# 15596018
Critical commercial assays		
EZ DNA Methylation-Gold Kit	ZYMO RESEARCH	Cat# D5005
KOD -Multi & Epi-	TOYOBO	Cat# KME-101
pEASY-Blunt Cloning Kit	TransGen Biotech	Cat# CB101-01
PrimeSTAR GXL DNA Polymerase	TAKARA	Cat# R050Q
SuperScript II Reverse Transcriptase	Invitrogen	Cat# 18064022
ChamQ Universal SYBR qPCR Master Mix	Vazyme	Cat# Q711-02
Dual-Luciferase® Reporter Assay System	Promega	Cat# E1910
LightShift® Chemiluminescent EMSA Kit	Thermo Scientific	Cat# 20148
Deposited data		
RNA seq data	This study	PRJCA016978
WGBS data	This study	PRJCA016978
Genome sequencing data for KD8-4C and KD8-4N	This study	PRJCA016978
Genome assemblies and annotations	This study	https://doi.org/10.57760/sciencedb.08245
Experimental models: Organisms/strains		
Rice: *Oryza sativa* ssp. *japonica* KenDao 8, KD8-N	This study	N/A
Rice: *Oryza sativa* ssp. *japonica* KenDao 8 acquired cold tolerance, KD8-C	This study	N/A
Rice: *Oryza sativa* ssp. *japonica* Shangyu 397, CS1	This study	N/A
Rice: *Oryza sativa* ssp. *japonica* Longdao 5, CT19	This study	N/A
Rice: Hybrid F_1, KD8-4N / KD8-4C	This study	N/A
Rice: *KD8-4N / ACT1 DM # 1*	This study	N/A
Rice: *KD8-4N / ACT1 DM # 2*	This study	N/A
Rice: *CS1 / ACT1 DM # 1*	This study	N/A
Rice: *CS1 / ACT1 DM # 2*	This study	N/A
Rice: *KD8-4C / ACT1 M # 1*	This study	N/A
Rice: *KD8-4C / ACT1 M # 2*	This study	N/A
Rice: *CT19 / ACT1 M # 1*	This study	N/A
Rice: *CT19 / ACT1 M # 2*	This study	N/A
Rice: *KD8-4C / ACT1 KO # 1*	This study	N/A
Rice: *KD8-4C / ACT1 KO # 2*	This study	N/A
Rice: *KD8-4C / ACT1 KO # 3*	This study	N/A
Rice: *KD8-4C / Dof1 KO #1*	This study	N/A
Rice: *KD8-4C / Dof1 KO #2*	This study	N/A
Rice: *KD8-4N / ACT1 OE # 1*	This study	N/A

(*Continued on next page*)

Continued

REAGENT or RESOURCE	SOURCE	IDENTIFIER
Rice: *KD8-4N / ACT1 OE # 2*	This study	N/A
Rice: *KD8-4N / Dof1-FLAG*	This study	N/A
Rice: *KD8-4C / Dof1-FLAG*	This study	N/A
Rice: *KD8-4N / CMT3 RNAi # 1*	This study	N/A
Rice: *KD8-4N / CMT3 RNAi # 2*	This study	N/A
Rice: *KD8-4N / MET1b RNAi # 1*	This study	N/A
Rice: *KD8-4N / MET1b RNAi # 2*	This study	N/A
Wild rice: P25; P46; GD-qy-01; IRGC 105882; IRGC 80546; VN01-16	Jing et al.[38]	N/A
Rice:31 varieties/landraces are listed in Table S1	National Mid-term GenBank for Rice of China National Rice Research Institute	N/A
Rice:131 landraces are listed in Table S3	National Mid-term GenBank for Rice of China National Rice Research Institute	N/A
Oligonucleotides		
Primers are listed in Table S4	Sangon Biotech	Custom order
Recombinant DNA		
ZmUbi: SunTag dCas9 TET1cd-ACT1	This study	N/A
ZmUbi: SunTag dCas9 DRM2cd-ACT1	This study	N/A
pCXUN-Cas9 ACT1	This study	N/A
ZmUbi: ACT1–FLAG	This study	N/A
$Actin1_{pro}$: CMT3 RNAi	This study	N/A
$Actin1_{pro}$: MET1b RNAi	This study	N/A
ZmUbi:Dof1–FLAG	This study	N/A
pYL-MH Dof1-	This study	N/A
Software and algorithms		
nextdenovo pipeline v2.2-beta.0.	Wang et al.[44]	https://github.com/Nextomics/NextDenovo
minimap2-nd v2.17-r941	Li[45]	https://github.com/lh3/minimap2
Trimmomatic v0.38	Bolger et al.[46]	https://github.com/usadellab/Trimmomatic
Nextpolish v1.1.0	Hu et al.[47]	https://github.com/Nextomics/NextPolish
RaGOO v1.1	Alonge et al.[48]	https://github.com/malonge/RaGOO.
BUSCO v4.0.2	Manni et al.[49]	https://gitlab.com/ezlab/busco
RepeatMasker v4.0.6	Smit et al.[50]	https://www.repeatmasker.org/
RepeatModeler v1.0.11	Smit and Hubley[51]	http://www.repeatmasker.org/RepeatModeler/
EDTA v1.8.3	Ou et al.[52]	https://github.com/oushujun/EDTA.
MAKER v3.01.02	Campbell et al.[53]	http://weatherby.genetics.utah.edu/CPB_MAKER/CPB_MAKER.tar.gz
hisat2 v2.1.0	Kim et al.[54]	http://daehwankimlab.github.io/hisat2/
SNAP v2006-07-28	Korf[55]	https://github.com/KorfLab/SNAP
Syri v1.1	Goel et al.[56]	https://github.com/schneebergerlab/syri
bwa v0.7.17-r1188	Li and Durbin[57]	https://github.com/lh3/bwa
GATK v4.2.3.0	McKenna et al.[58]	http://www.broadinstitute.org/gsa/wiki/index.php/The_Genome_Analysis_Toolkit
bedtools v2.29.1	Quinlan and Hall[59]	http://code.google.com/p/bedtools
Stringtie v1.3.4d	Kovaka et al.[60]	https://github.com/gpertea/stringtie
sva package (v3.50.0)	Leek et al.[61]	https://bioconductor.org/packages/release/bioc/html/sva.html
pheatmap (v1.0.12)	Kolde[62]	https://github.com/raivokolde/pheatmap

(*Continued on next page*)

Continued

REAGENT or RESOURCE	SOURCE	IDENTIFIER
ggplot2 (v3.5.0)	Hadley[63]	https://ggplot2.tidyverse.org/
DESeq2 v1.34.0	Love et al.[64]	http://www.bioconductor.org/packages/release/bioc/html/DESeq2.html
Bismark (v0.19.1)	Krueger and Andrews[65]	www.bioinformatics.bbsrc.ac.uk/projects/bismark/
methylKit (version 1.8.1)	Akalin et al.[66]	http://code.google.com/p/methylkit.
bowtie (v1.3.1)	Langmead and Salzberg[67]	http://bowtie.cbcb.umd.edu.
ShortStack (v4.0.2)	Axtell[68]	http://axtell-lab-psu.weebly.com/shortstack.html.

EXPERIMENTAL MODEL AND STUDY PARTICIPANT DETAILS

Plant materials and growth conditions

All rice plants (*Oryza sativa L.*) used in this study were grown in natural conditions (except for 7-d cold treatments done at the booting stage) either in Harbin (126°37'11"E, 45°41'00"N), China, from May to October in long-day conditions, or in Lingshui (110°0'30"E, 18°32'8"N), China, from December to April in short-day conditions from 2014 to 2024. These rice landraces were randomly selected based on the province information from the National Mid-term GenBank for Rice of the China National Rice Research Institute.

METHOD DETAILS

Plant cold treatment

Cold treatment at the booting stage was performed annually in Harbin from July to September using a phytotron (Koito, Japan) under natural lighting conditions. Each plant was grown in a cylindrical plastic pot 15 cm in height and 12 cm in diameter containing local soil in the natural environment until cold treatment. During the booting stage, the tillers with the auricle distance between the flag leaf and the penultimate leaf of –5 cm to –2 cm, which were considered to have panicles where most florets were at the meiosis stage, were tagged and the whole plant was moved to a phytotron for cold treatment (15°C constant temperature). After cold treatment for 7 d, plants were returned to the natural environment until maturity. The ratios of stained pollen or seed setting from the tagged tillers were measured to evaluate the cold tolerance of each plant. Mature pollen grains were stained as previously described.[69]

Generation of transgenic rice plants

Previously published epigenome-editing vectors were used to generate targeted *ACT1* demethylation lines in the KD8 background.[29] Two fragments of *U6 ACT1*-sgRNA for epigenome editing were amplified using primers of CF6964/CF8415 and CF8414/CF6965 from the *U6* template vector. The two fragments were inserted into the *Pme*I-digested Zmubi-SunTag-14aa vector using Gibson assembly.

To generate targeted DNA-methylation editing system, we amplified the *Nicotiana tabacum* DRM2 catalytic domain using primer pairs XP0020 and XP0021. The amplified fragment was inserted into the ZmUbi: SunTag dCas9 TET1cd-ACT1 vector digested by the *BsiW*I to replace the TET1 catalytic domain.

ACT1 knockout lines were generated in the KD8-4C background by CRISPR–Cas9. The gene-editing vector was constructed according to a previous study.[70] In brief, two fragments of *U3 ACT1*-sgRNAs were amplified using primers OsU3-F/ACT1-R and ACT1-F/OsU3-R from the *U3* template vector then inserted into *Kpn*I-digested pCXUN-Cas9 vector using Gibson assembly. The *ACT1* over-expression lines driven by maize *UBIQUITIN* promoter were generated in the background of KD8-4N. The full-length *ACT1* coding sequence was amplified using CF9200 and CF9201 primers and the PCR fragment was inserted into the *Sac*I/*BamH*I-digested XF2753 vector using Gibson assembly. To mutate *Dof1*, two gene-editing targets were designed and inserted into the pYLCRISPR/Cas9Pubi-H binary vector as previously described.[71]

To generate the *ZmUBI*$_{pro}$*:Dof1–FLAG* over-expression vector, fragments containing the *Dof1* coding sequence and *3xFLAG* tag were obtained using primers XP3067 and XP3068 using plasmid XF2753 as template, and the amplified products was inserted to the pCXUN backbone digested by *Bam*HI using Gibson Assembly.

The *CMT3* and *MET1b* RNAi lines were generated in the KD8-4N background. The RNAi vector was constructed as previously described.[72] Fragments to target *CMT3* and *MET1b* were obtained using primers CF8768/CF8769 and CF8770/8771, respectively.

Agrobacterium-mediated transformation and regeneration of plants were performed as previously reported with minor modifications.[73] Primers for constructs are listed in Table S4 in supplemental information.

Total RNA isolation and qRT–PCR analysis

Total RNA was extracted from panicles at the booting stage with TRIzol reagent (15596018; Invitrogen). First-strand cDNA was synthesized from 2 μg of total RNA using Superscript II Reverse Transcriptase (#18064022; Invitrogen). Ten-fold-diluted cDNA samples were used as template for real-time qPCR analysis using Bio-Rad CFX Manager with ChamQ Universal SYBR qPCR Master Mix (Q711-02; Vazyme). The expression levels of target genes were normalized against *UBIQUITIN* (*LOC_Os03g13170*). Each data point includes at least three biological replicates. Primers for qRT–PCR and real-time PCR are listed in Table S4 in supplemental information.

PCR amplification with methylation-sensitive restriction enzyme (Chop–PCR)

Genomic DNA was extracted using a CTAB method and 500 ng was digested with methylation-sensitive restriction enzyme *Aci*I (R0551V; New England Biolabs) overnight at 37°C and followed by PCR amplification. Chop–PCR primers are listed in Table S4 in supplemental information.

Bisulfite-sequencing-based DNA-methylation analysis

Bisulfite treatment was conducted using the EZ DNA Methylation-Gold Kit (D5005; Zymo Research) according to the instruction manual. Bisulfite-treated DNA was used to amplify the target regions using primers listed in Table S4. PCR products were purified and cloned into pEASY-Blunt vector (CB101-01; TransGen Biotech) for sequencing. The sequencing results were analyzed with Kismeth software[74] and the methylation percentages of each cytosine site were calculated.

For detection of DNA-methylation levels by amplicon deep sequencing, the bisulfite-treated genomic DNA was used as a template followed by two rounds PCR. In the first PCR, the target region was amplified using site-specific primers. In the second PCR, both forward and reverse barcodes were added to the ends of the PCR products for library construction.[75] Equal amounts of PCR products were pooled and samples were sequenced (Annoroad Gene Technology, Novaseq 6000 platform). The sequencing data were analyzed by HiMeth (http://www.hi-tom.net/Hi-TOM_meth/).

EMSA

Recombinant MBP–Dof1 and MBP were incubated with biotin-labeled probes, competitor probes, or mutant probes, using a LightShift Chemiluminescent EMSA kit (20148, Thermo Fisher), on ice for 60 min. Binding reactions were terminated by adding 5× native sample-loading buffer, and samples were separated by native PAGE. Binding signal was detected using a Nucleic Acid Detection Module kit (89880, Thermo Fisher).

ChIP–qPCR assay

ChIP assays were performed as previously described with minor modifications.[76] Briefly, approximately 1 g of *Dof1* overexpression line seedlings were crosslinked, and chromatin was extracted and sonicated to obtain DNA fragments. DNA fragments associated with Dof1–FLAG were incubated with anti DDDDK-Tag antibody (AE092, ABclonal). Enriched DNA fragments were collected with a ChIP DNA Clean and Concentrator kit (D5205, ZYMO). The immunoprecipitated DNAs were quantified by qPCR with the primers specific to target regions. The fold enrichment is indicated by the ratio of ChIP DNA to input DNA.

Transcriptional activity assay

To investigate the transactivation activity of Dof1, a dual-luciferase reporter assay was used with transiently transgenic rice protoplasts. The full-length sequence of *Dof1* was obtained by PCR using primers CF9351 and CF9352. The *GAL4* DNA-binding domain (BD) coding sequence was fused to *Dof1* and inserted into pRT107 to generate GAL4–Dof1 effector plasmids. The fusion genes were under the control of *35S* promoter. The BD sequence was also fused to *VP16* to generate a positive control effector plasmid. pRT107 containing the BD sequence was used as negative control. The reporter plasmid containing *5xUAS* and *35S* promoter upstream of a reporter gene encoding a firefly luciferase (LUC) was used. The effector and reporter plasmids were co-transfected into rice protoplasts.[77] Protoplasts derived from 14-d-old etiolated seedlings were co-transformed with reporter and control plasmids. *35S:REN* was used as an internal control. Total proteins were extracted from the samples using dual-LUC assay reagents. The LUC/REN ratio was employed to quantify the relative promoter activity of *Dof1*, as measured with a GloMax 20/20 luminometer.

Genome sequencing, assembly and annotation

Genomes were sequenced with Oxford Nanopore Technology (ONT) at Nextomics Biosciences and NovaSeq at BerryGenomics. For genome assembly, ONT long reads were *de novo* assembled with nextdenovo pipeline v2.2-beta.0.[44] Firstly, nextcorrect was used to correct sequencing errors. The minimum-length threshold for seed sequences for KD8-4C and KD8-4N was determined to be 28,121 bp and 30,278 bp. Seed sequences were then extracted with seq_dump and transformed to bit format with seq_bit. By aligning ONT long reads to seed sequences with minimap2-nd v2.17-r941,[45] overlaps between ONT reads and seed sequences, as well as dovetail overlaps between seed sequences, were identified. Reads were corrected based on consensus-overlap results. Secondly, corrected reads were assembled with nextgraph with parameters "-a 1 -n 438 -Q 7 -I 0.35 -S 0.18 -N 1 -r 0.39 -m 5.29 -C 99 -z 16."

For genome polishing, chromosome assembly, and evaluation, short reads were firstly cleaned before use in genome polishing. Adaptors and low-quality bases were trimmed using Trimmomatic v0.38[46] with parameters "ILLUMINACLIP: MGISeq.fa:0:30:10 LEADING:3 TRAILING:3 CROP:145 HEADCROP:10 SLIDINGWINDOW:4:20 MINLEN:75." Nextpolish v1.1.0,[47] was then used to

correct possible errors in assembly. Briefly, ONT reads were firstly mapped to genomes and error corrections were performed with parameters "task=1212; lgs_options = -min_read_len 10k -max_read_len 150k -max_depth 60" for two iterations. Secondly, clean short reads were mapped to the corrected genome and further polishing was performed with parameters " task=1212; sgs_options= -max_depth 100." with three iterations. Contigs were further anchored to chromosomes using homology information between draft assemblies and Nipponbare assembly (IRGSP1.0) with RaGOO v1.1.[48] Genome completeness was performed with BUSCO v4.0.2[49] using 425 BUSCO groups from clade Viridiplantae.

For genome annotation, transposable elements were first identified using a combination of homology and *ab initio* approaches. For the homology-based approach, RepeatMasker v4.0.6[50] was used to predict transposable elements with known rice transposable-element library with species "rice." For the *ab initio*-based approach, RepeatModeler v1.0.11[51] (http://repeatmasker.org/RepeatModeler/) was used to build a transposable-element library for KD8-4C and KD8-4N and RepeatMasker v4.0.6 for identifying transposable elements with an *ab initio* library.[78] Both results were merged and used for genome masking before gene prediction. For intact transposable elements, EDTA v1.8.3[52] was used for identifying DNA transposons and LTR retrotransposons.

After masking repetitive elements, MAKER v3.01.02 pipeline was adopted to annotate the gene structure in the genomes of KD8-4C and KD8-4N.[53] Transcription and homology evidence were first prepared. RNA-seq reads of newly generated libraries as well as published libraries of roots, leaves, and spikelets from Stein et al., were aligned to the genomes of KD8-4C and KD8-4N with hisat2 v2.1.0.[54,79]

For homology evidence, we downloaded protein sequences from rice (IRGSP1.0),[80] maize (AGPv4),[81] Arabidopsis (TAIR10)[82] and curated protein sequences from Uniprot-Swissprot with clade Viridiplantae (accessed 11 December, 2019).

These evidences were subsequently compiled and utilized in gene annotation through an iterative approach. For the first round of gene annotation, we inferred gene structures directly from transcript and protein evidence with "est2genome=1 and protein2genome=1". The predicted genes were used to train *de novo* gene predictors Augustus v3.3.3 and SNAP v2006-07-28.[55] For the second round, we used the trained models of SNAP and Augustus to predict genes and integrated results with maker v3.01.02, obtaining the final annotation.[53] A total of 35,545 and 35,925 genes were annotated for KD8-4C and KD8-4N. Orthologs between KD8-4C, KD8-4N, and Nipponbare (IRGSP1.0) were identified with getRBH.pl (https://github.com/ComputationalconSequences/ Sequence Tools /blob /master/getRBH.pl).

Identification of variation between KD8-4C and KD8-4N genomes

Two approaches were used to identify variation between KD8-4C and KD8-4N. An assembly-based approach was first used to identify variations between chromosome assemblies with Syri v1.1.[56] Even though careful curations were performed during the assembly step, it is still possible that the resulting assembly could contain assembly errors, which could affect the identification of variations between the two assemblies. Therefore, we took a stringent pipeline to filter raw SNPs and Indels identified by Syri. Clean short reads for KD8-4C and KD8-4N were mapped back to the respective genome with bwa mem v0.7.17-r1188.[57] Bedtools multicov v2.29.1[59] was then used to calculate read depth and only variations with depth over 20 were retained. The read-mapping-based approach was performed by applying the best practice of GATK v4.2.3.0[58] to bam files generated by bwa. Briefly, duplicated reads were first masked with gatk MarkDuplicates.[83] gatk HaplotypeCaller[83] was then used to generate raw gvcfs, which were then used for genotyping with gatk GenotypeGVCFs. Identified SNPs were filtered with crieteria "QD < 2.0 || MQ < 40.0 || FS > 60.0 || SOR > 3.0 || MQRankSum < -12.5 || ReadPosRankSum < -8.0" with gatk VariantFiltration. Identified Indels were filtered with criteria "QD < 2.0 || FS > 200.0 || SOR > 10.0 || MQRankSum < -12.5 || ReadPosRankSum < -8.0" with gatk GenotypeGVCFs. SNPs and indels that were identified in both the assembly-based and read-mapping-based approaches were considered as high-quality variations and retained. The locations of variations were identified with bedtools intersection v2.29.1.[59] Identified missense mutations were further verified using PCR and Sanger sequencing and were retained after they passed validation.

Transcriptome analysis

Strand-specific RNA-seq reads of KD8-4C, KD8-4N, and F_1 transcriptomes were mapped to the Nipponbare reference genome (IRGSP1.0)[80,83] with HiSAT2 v2.1.0[54] with parameters "–rna-strandness RF –mp 3,1." For coverage plot, regions of interest were tiled into windows of 20 bp and FPKMs for each window were first calculated:

$$FPKM = \frac{WindowMappedFragments \times 10^9}{TotalMappedFragments \times WindowSize}$$

Average FPMKs were then taken from different replicates and visualized using IGV (v2.16.0).[84] Expression abundance for each gene was quantified using Stringtie v1.3.4d.[60] Batch effects were corrected using ComBat_seq in sva package (v3.50.0).[61] Corrected Transcripts Per Million (TPMs) were visualized in the heatmap and principal-component analysis (PCA) using pheatmap (v1.0.12)[62] and ggplot2 (v3.5.0).[63] Differentially expressed genes with at least two-fold expression change and a Benjamini–Hochberg adjusted p value < 0.05 (Wald test) were identified with DESeq2 v1.34.0.[64] Genes with maximum corrected TPM values below 15 were excluded as lowly expressed. Based on the dominant nature of the acquired cold-tolerance trait, candidate genes would show similar expression patterns between KD8-4C and F_1 progeny, but different from KD8-4N, when responding to cold stress. Following this assumption, 188, 142 and 1,544 genes were identified at 1-, 3-, and 5-d cold-treatment time points, respectively, with 12 genes common to all three time points. Meiosis in rice young panicles takes longer due to the different developmental stages of florets, particularly under

low-temperature conditions. Genes with prolonged differential expression are likely candidates, so we focused on these 12 genes. After cold treatment of day 1, day 3, and day 5, candidate genes that were consistently down-regulated in KD8-4N but unchanged in KD8-4C and F_1 were identified as Set A, genes that were consistently up-regulated in KD8-4N but unchanged in KD8-4C and F_1 were identified as Set B, genes that were consistently down-regulated in KD8-4C and F_1 but unchanged in KD8-4N were identified as Set C, genes that were consistently up-regulated in KD8-4C and F_1 but unchanged in KD8-4N were identified as Set D, genes that were consistently down-regulated in KD8-4N but up-regulated in KD8-4C and F_1 were identified as Set E, and genes that were consistently up-regulated in KD8-4N but down-regulated in KD8-4C and F_1 were identified as Set F.

Whole-genome bisulfite-sequencing data processing

Clean reads from whole-genome bisulfite sequencing (WGBS) of KD8-4C and KD8-4N were mapped to the Nipponbare reference genome (IRGSP 1.0)[80,83] for each sample using Bismark (v0.19.1) pipeline with Bowtie2 and default parameters.[65,67] Duplicated reads were then removed using the script deduplicate_bismark. The methylation information of every single cytosine site was called from the uniquely mapped reads using bismark_methylation_extractor implemented in Bismark. The bisulfite non-conversion rate was estimated from the total number of cytosine (Cs) divided by the total coverage of cytosines and thymines (Cs and Ts) by mapping WGBS reads onto the unmethylated chloroplast genome.

For DNA-methylation analysis, gene bodies or transposable elements were equally divided into 60 bins, and 2-kb upstream or downstream of each gene body or transposable element were divided into 20 bins, with 100 bp in each bin. The average methylation level was calculated for each bin and plotted. The average methylation levels for CG, CHG, and CHH contexts were calculated, respectively, by the formula [Cs/ (Cs + Ts) * 100], where Cs and Ts represent total cytosine (methylated) and thymine (unmethylated) read counts.

Identification of differentially methylated regions

Differentially methylated regions were identified by comparing the methylation level of 100-bp windows throughout the whole genome between KD8-4C and KD8-4N lines using methylKit (version 1.8.1) pipeline.[66] Briefly, regions were defined by tiling the genome into 100-bp bins with 50-bp as the step size and comparing the number of called Cs and Ts in each sample. To avoid 100-bp bins with few cytosines, only bins with at least five cytosines that are covered by at least five reads in each sample were selected for further analysis. Bins with a methylation difference of 0.3 for CG, CHG, and CHH contexts and a Benjamini–Hochberg adjusted p value < 0.01 (Fisher's exact test) were selected as candidate differentially methylated regions. Finally, candidate regions within 200 bp of each other were merged as final differentially methylated regions because loss and gain of methylation occurs in clusters. Regions were annotated into four groups including those located within gene promoters, within gene bodies, within transposable elements, and in intergenic regions. Differentially methylated regions located in multiple groups are only counted once with descending priorities of the promoter, gene body, transposable element, and intergenic.

Characterization of the *ACT1* locus

Upon exposure to cold stress, 12 candidate genes were identified that exhibited similar expression patterns between KD8-4C and the F_1 progeny, but differed from expression in KD8-4N. Specifically, 11 genes were found to be down-regulated ($\log_2$FC < −1, Benjamini–Hochberg adjusted p value < 0.05, Wald test) in KD8-4N but not in KD8-4C and the F_1 progeny (designated as Set A), while one genes were up-regulated in KD8-4N ($\log_2$FC > 1, Benjamini–Hochberg adjusted p value < 0.05, Wald test) but not in KD8-4C and the F_1 progeny (designated as Set B), in response to cold stress. Subsequently, we examined mutations in the promoters of these genes and determined that there were no DNA differences in the promoters between KD8-4C and KD8-4N. Finally, we identified differentially methylated regions (DMR) with methylation difference > 0.3 and Benjamini–Hochberg adjusted p value < 0.01 using Fisher's exact test. We screened these DMRs in the promoter regions (2 kb upstream of ATGs) of the twelve expression changed genes and revealed: *ACT1*, a Set-A gene, exhibited hypomethylation in KD8-4C compared to KD8-4N.

Small-RNA analysis

Small RNAs were aligned to the Nipponbare genome (IRGSP1.0)[83] with bowtie (v1.3.1).[85] Up to 50 valid alignments for each read were retained with at most one mismatch allowed for each alignment. Loci of small RNAs are annotated using ShortStack (v4.0.2).[68] Initial clusters were first identified based on coverage of alignment result, and overlapping clusters were merged with flanking 75 bp with the option "–pad 75". Loci of small RNAs with size ranges from 20–24 nt were then identified with the strandedness cutoff of 0.8 and expressions were quantified. For 24-nt small RNA loci, their targeting of differentially methylated regions was identified with bedtools intersection v2.29.1.[59]

QUANTIFICATION AND STATISTICAL ANALYSIS

Statistical analysis was performed with Graphpad Prism 8 (https://www.graphpad.com/scientific-software/prism/). Ordinary two-way ANOVA, one-way ANOVA and Student's t-test were used to obtain P values and different letters or asterisks above bars represent the significant difference at p < 0.05. The details of experiments are in respective figure legends.

CellPress
OPEN ACCESS

Supplemental figures

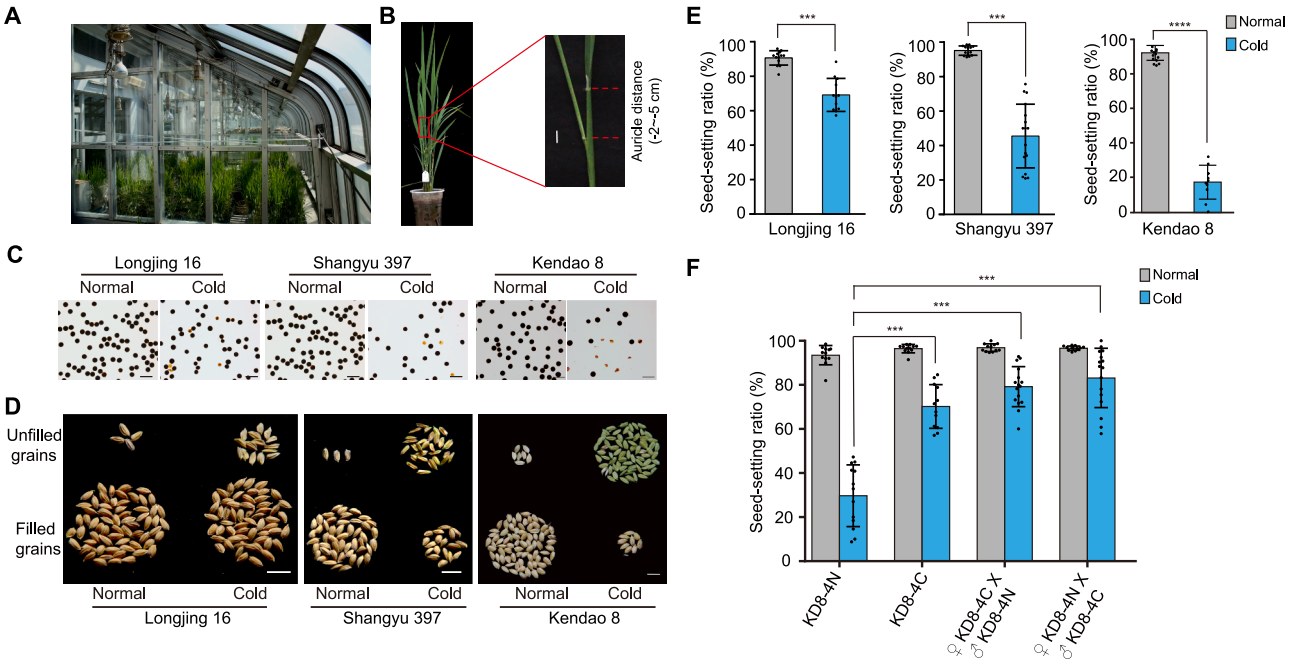

Figure S1. Evaluation system for rice cold tolerance at meiotic stage, related to Figure 1

(A) Exerting cold stress on meiotic rice in temperature-controlled growth chambers.

(B) Meiotic-stage determination by auricle distance between FLAG leaf and penultimate leaf. Panicles with auricle distances of −2 to −5 cm were used for cold-tolerance evaluation. Scale bar, 2 cm.

(C–E) Phenotypes of pollen fertility determined by potassium-iodide staining (C), filled or unfilled grains of a representative panicle (D), and seed-setting ratio (E) of three rice varieties with different cold tolerance grown at normal and cold temperatures. Scale bars, 100 μm (pollen) and 1 cm (grain). ***$p < 0.001$, ****$p < 0.0001$; Wilcoxon matched-pairs signed rank test.

(F) Seed-setting ratio of KD8-4N, KD8-4C, and their reciprocally crossed F_1 progenies grown under normal and cold temperatures. ****$p < 0.0001$, ***$p < 0.001$; Wilcoxon matched-pairs signed rank test.

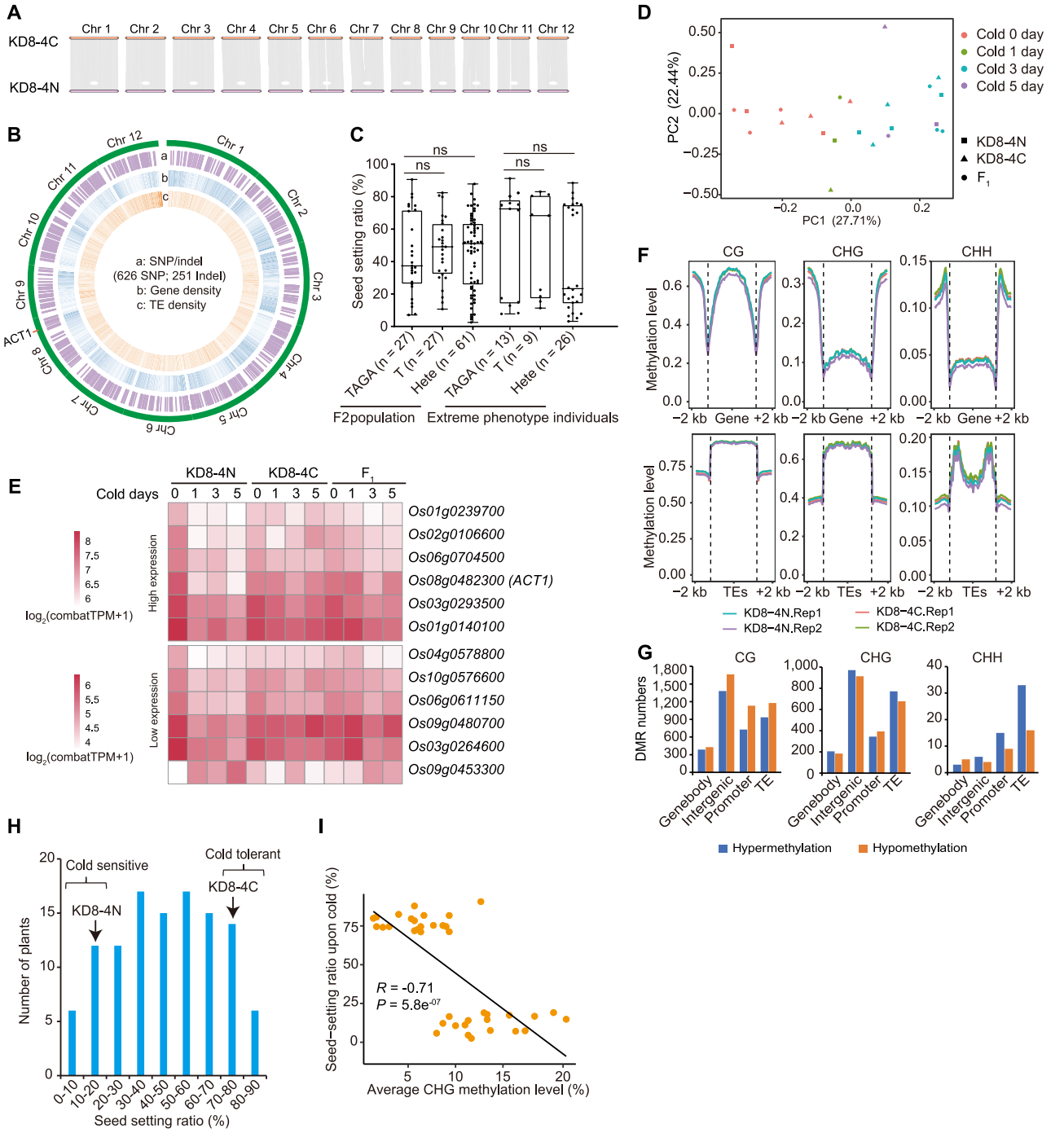

Figure S2. Comparative multi-omics analysis between KD8-4N and KD8-4C aimed at identifying candidate causal genes for acquired cold tolerance, related to Figure 2

(A) Syntenic analysis of KD8-4N and KD8-4C genomes.

(B) Overview of the assembled KD8-4N genome including (a) SNPs/indels between KD8-4N and KD8-4C genomes, (b) density of genes, and (c) distribution of transposon elements.

(C) Seed-setting ratio of progenies with different genotypes for the only indel (chr2: 33,482,848) that leads to an altered amino acid sequence, among the F_2 population generated by reciprocal crosses between KD8-4N and KD8-4C, and the extreme-phenotype F_2 progenies. Hete, heterozygous. Statistically significant differences are indicated by different lowercase letters. Kruskal-Wallis test with Dunn's multiple comparisons test, $p < 0.01$.

(D) Principal-component analysis of meiotic-stage panicles transcripts per million (TPMs) from KD8-4N, KD8-4C, and their F_1 at different cold-treatment time points.

(legend continued on next page)

(E) Heatmap of expression profiles for the 12 candidate genes in cold treatment days 0, 1, 3, and 5 in KD8-4N, KD8-4C, and their F_1. Mean TPM is used for treatments with multiple replicates.
(F) Genome-wide levels of methylated cytosine in sequence contexts of CG, CHG, and CHH of genes and transposable elements, each with their contiguous upstream and downstream 2-kb flanking regions in KD8-4N and KD8-4C.
(G) Hyper- or hypomethylation differentially methylated region numbers for each sequence context (CG, CHG, and CHH) in gene bodies, intergenic regions, promoters, and transposable elements between KD8-4N and KD8-4C.
(H) Frequency distribution of seed-setting ratio upon cold treatment in the F_2 population from a cross between KD8-4N and KD8-4C.
(I) Scatterplot showing the linear correlation between *ACT1* DNA methylation (CHG) and seed-setting ratio among the progenies from F_2 populations of KD8-4N and KD8-4C. Statistical significance of the correlation is determined by Pearson's product-moment correlation. *R*, Pearson's correlation coefficient.

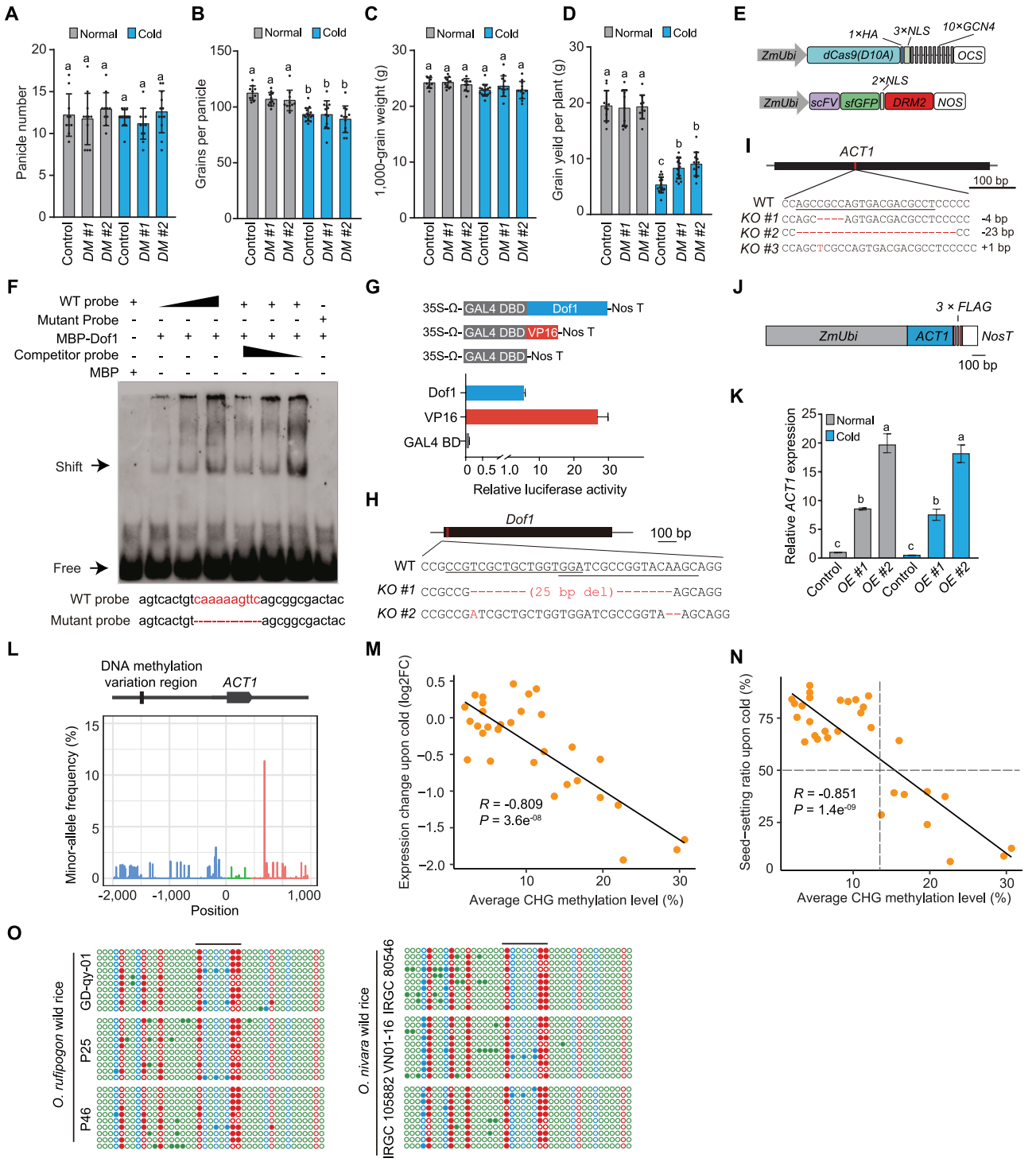

Figure S3. Genetic analysis confirming DNA-methylation changes in *ACT1* that confer acquired cold tolerance, related to Figures 3 and 4

(A–D) Quantification of agronomic traits for negative control, *DM #1*, and *DM #2* plants grown under normal and cold temperatures: (A) panicle number; (B) grains per panicle; (C) 1,000-grain weight; (D) grain yield per plant. Statistically significant differences are indicated by different lowercase letters. One-way ANOVA with Tukey's multiple comparisons test, $p < 0.01$.

(E) Schematic of the SunTag-dCas9-DRM2 DNA-methylation system. *ZmUbi*, *Zea mays ubiquitin* promoter; *dCas9*, nuclease-inactive Cas9; *NLS*, nuclear-localization signal; *GCN4*, yeast transcription factor GCN4 preserving the binding site for the scFv; *scFv*, single-chain antibody fragment; *DRM2*, *Nicotiana tabacum* DRM2 catalytic domain; *HA*, human influenza hemagglutinin epitope tag; sfGFP, superfolder green fluorescent protein; *OCS*, octopine synthase terminator; *NOS*, nopaline synthase terminator.

(legend continued on next page)

(F) EMSA showing MBP-Dof1 binding *in vitro* to wild-type motif in the *ACT1* promoter but not to the mutated motifs.
(G) Top: constructs used for transient dual-reporter expression assays. The transcriptional activation ability of Dof1 was probed by co-expressing *GAL4-Dof1* and the reporter construct $35S_{pro}$*:REN* $GAL4_{pro}$*:LUC*.
(H) Diagram of CRISPR-Cas9-generated *Dof1* alleles in the KD8-4C background. The guide RNA target sequences are underlined. Red dashes and red letters indicate the deletion and insertion nucleotides in *Dof1* knockout lines (*KO #1*, *KO #2*), respectively.
(I) Diagram of CRISPR-Cas9-generated *ACT1* alleles in the KD8-4C background. The guide RNA target sequences are underlined. Red dashes and red letters indicate the deletion and insertion nucleotides in *ACT1* knockout lines (*KO #1–3*), respectively.
(J) Diagram of the *ACT1-3xFLAG* construct used for overexpression in the KD8-4N background.
(K) *ACT1* expression in KD8-4N control and two *ACT1-3xFLAG* transgenic lines (*OE #1*, *OE #2*) grown under normal and cold conditions. Statistically significant differences are indicated by different lowercase letters. One-way ANOVA with Tukey's multiple comparisons test, $p < 0.01$.
(L) Minor-allele frequency analysis of *ACT1* among 2,847 sequenced Asian cultivated rice accessions from the 3,000 Rice Genomes Project.
(M and N) Correlations between DNA-methylation level (CHG) and *ACT1* expression changes upon cold (M); *ACT1* DNA-methylation level (CHG) and seed-setting ratio (N) in 31 rice varieties/landraces. The dotted lines in (N) indicate the thresholds of cold-sensitive/tolerant groups or low/high DNA-methylation groups. Statistical significance of correlations was determined by Pearson's correlation coefficient. *R*, Pearson correlation coefficient.
(O) Bisulfite sequencing of the *ACT1* region in wild rice accessions.

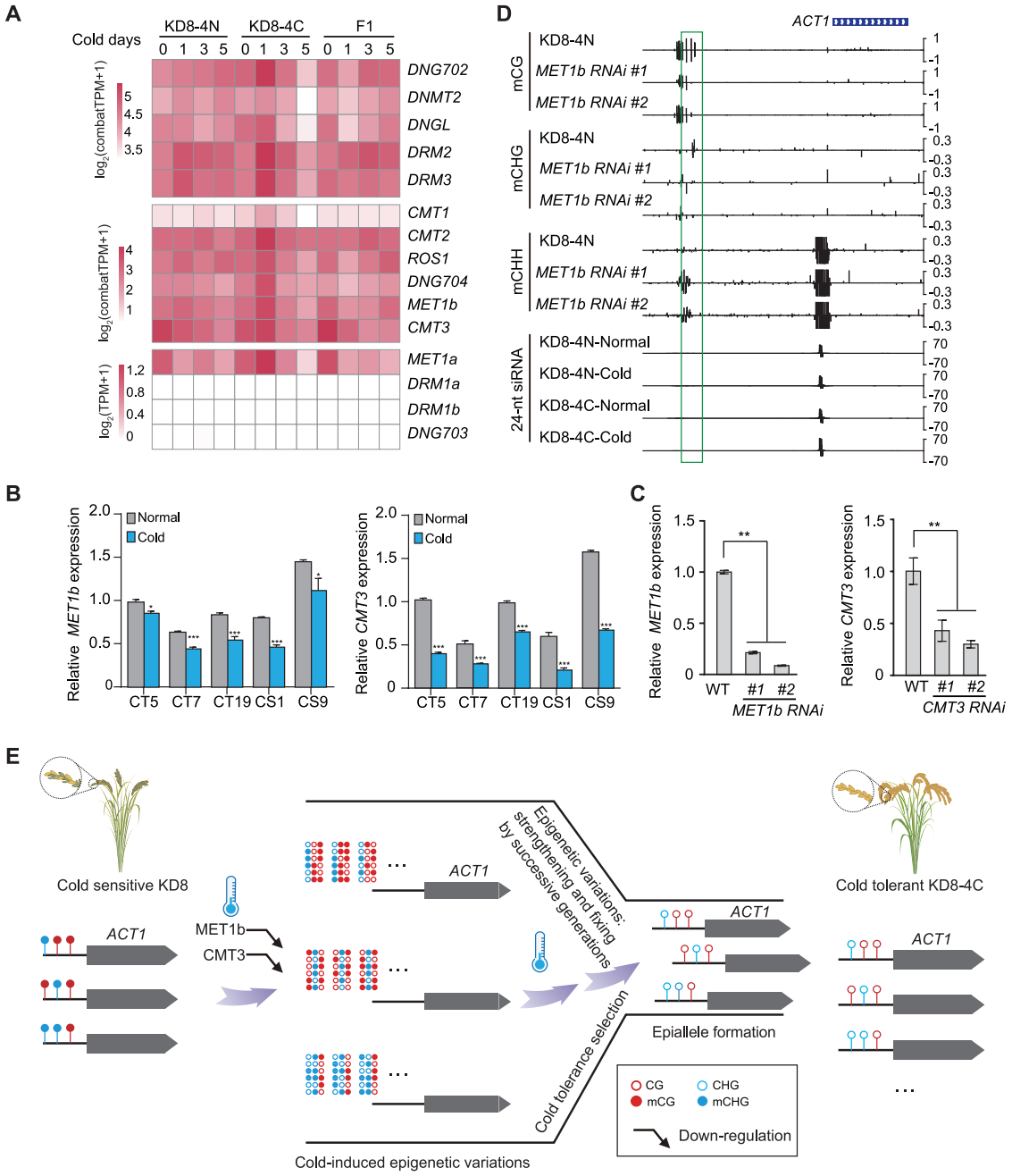

Figure S4. Proposed mechanism for cold-induced DNA-methylation variation mediating adaptive cold-tolerant acquisition, related to Figure 4

(A) Heatmap showing expression levels of 10 DNA methyltransferase and 5 demethylase genes in KD8-4N, KD8-4C, and their F_1 at the indicated cold-treatment time points.

(B) RT-qPCR analysis of *CMT3* and *MET1b* in different rice varieties at normal and cold conditions. *UBIQUITIN* was used to normalize relative expression. Values are means ± SD of three biological replicates. $^{*}p < 0.05$, $^{***}p < 0.001$; Student's t test.

(C) Relative expression of *MET1b* and *CMT3* in WT and RNAi lines. *UBIQUITIN* was used to normalize relative expression. Values are means ± SD of three biological replicates. $^{**}p < 0.01$, one-way ANOVA with Tukey's multiple comparisons test.

(D) Genome-browser view of DNA methylation and 24-nt siRNA abundance at the *ACT1* region in KD8-4N, KD8-4C, and *MET1b* RNAi lines.

(E) Proposed working model of cold-induced DNA-methylation variation mediating adaptive cold-tolerant acquisition.